PHYSICAL REVIEW D **83,** 115012 (2011)

Momentum reconstruction at the LHC for probing *CP* violation in the stop sector

G. Moortgat-Pick,[1,3,*] K. Rolbiecki,[2,3,†] and J. Tattersall[2,4,‡]

[1]*II. Institut für Theoretische Physik, University of Hamburg, Luruper Chaussee 149, D-22761 Hamburg, Germany*
[2]*IPPP, University of Durham, Durham DH1 3LE, UK*
[3]*DESY, Deutsches Elektronen-Synchrotron, Notkestrasse 85, D-22607 Hamburg, Germany*
[4]*Bethe Centre for Theoretical Physics and Physikalisches Institut, Universität Bonn, D-53115 Bonn, Germany*

(Received 5 October 2010; published 10 June 2011)

We study the potential to observe *CP*-violating effects in supersymmetric $\tilde{t}_1$-cascade decay chains at the LHC. Asymmetries composed of triple products of momenta of the final-state particles are sensitive to *CP*-violating effects. Because of large boosts that dilute the asymmetries, these can be difficult to observe. If all particle masses in a cascade decay are known, it may be possible to reconstruct all momenta in the decay chains on an event-by-event basis even when we have missing momentum due to a stable lightest supersymmetric particle. After the reconstruction, the nondiluted *CP*-violating signal can be recovered and gets significantly enhanced so that an observation may become feasible. A fully hadronic study has been completed to define the areas of the minimal supergravity parameter space that may yield a 3-σ observation with 500 fb^{-1} at the LHC.

DOI: 10.1103/PhysRevD.83.115012 PACS numbers: 14.80.Ly, 11.30.Er, 12.60.Jv

I. INTRODUCTION

The minimal supersymmetric standard model (MSSM) is a particularly compelling extension of the standard model (SM), that may soon be explored at the Large Hadron Collider (LHC). It allows one to stabilize the hierarchy between the electroweak (EW) scale and the Planck scale and to naturally explain electroweak symmetry breaking (EWSB) by a radiative mechanism. The naturalness of the scale of electroweak symmetry breaking and the Higgs mass places a rough upper bound on the superpartner masses of several TeV and the fits to the electroweak precision data point to a rather light supersymmetry (SUSY) spectrum [1]. If supersymmetry is discovered, many studies will be required to determine the exact details of its realization. One of the interesting issues in this context is *CP* violation. While the observed amount of *CP* violation in the *K* and *B* sectors can be accommodated within the SM, another piece of evidence, the baryon asymmetry of the Universe, requires a new source of *CP* violation [2–4].

The MSSM contains 105 free parameters [5] and a large number of these may have nonzero *CP*-violating phases; see e.g. Ref. [6]. Many of the phases are unphysical in the sense that they can be rotated away by a redefinition of the fields. The parameters normally chosen to be complex and relevant to this study are the $U(1)$ and $SU(3)$ gaugino mass parameters M_1 and M_3, the Higgsino mass parameter μ, and the trilinear couplings of the third generation sfermions A_f ($f = b, t, \tau$). Hence we have

$$M_1 = |M_1|e^{i\phi_1}, \qquad M_3 = |M_3|e^{i\phi_3},$$
$$\mu = |\mu|e^{i\phi_\mu}, \qquad A_f = |A_f|e^{i\phi_{A_f}}. \tag{1}$$

The two complex parameters that enter the $\tilde{t}$ sector at tree level are A_t and μ and in the $\tilde{\chi}_i^0$ sector μ and ϕ_1. Certain combinations of the *CP*-violating phases of these parameters are constrained by the experimental upper bounds on various electric dipole moments (EDMs); see e.g. Ref. [7]. Ignoring possible cancellations, the most severely constrained phase is that of μ which contributes to the EDMs at the one-loop level. In general for $\mathcal{O}(100)$ GeV supersymmetric masses, $|\phi_\mu|$ has to be very small and we therefore set $\phi_\mu = 0$ throughout our study. The phase of A_t has weaker constraints as it only contributes to the EDMs at the two-loop level [8–14]. Here we study the complete range of ϕ_{A_t} in order to see the general dependencies exhibited by our observables and the luminosity required to observe this within the LHC environment. In principle, ϕ_1 can also contribute to our observables but in the minimal supergravity (mSUGRA) scenarios discussed in this paper, the dependence is weak due to the wino character of the $\tilde{\chi}_2^0$. We would like to stress that in the chosen scenario experimental bounds from EDMs can be evaded by arranging cancellations between various supersymmetric contributions for any value of A_t [7,15–17].

In general *CP* phases alter the couplings and masses of SUSY particles; see Ref. [18] for a recent review at the LHC. Therefore, in principle we could detect *CP*-violating effects by studying mass spectra, cross sections, and branching ratios [19,20]. However, to interpret these measurements accurately, we will require high precision and will rely on many assumptions of the underlying SUSY-breaking mechanism. In addition, all of these observables are *CP*-even and can be faked by a multitude of other parameters.

*gudrid.moortgat-pick@desy.de
†krzysztof.rolbiecki@durham.ac.uk
‡jamie.tattersall@durham.ac.uk

In order to make the unambiguous observation of a complex parameter, we need to use CP-odd observables. Examples of CP-odd observables include rate asymmetries of cross sections and branching ratios. Another possibility, however, are observables that are odd under T-transformations. Applying CPT-invariance, T-odd observables can be transferred under certain conditions into CP-odd variables; see Sec. II B. These kinds of observables can be defined using the triple product correlations of momenta that are based on spin correlations of particles; see Refs. [21,22] for a recent review. For the case of SUSY at the LHC, we can do this using the final-state particles of cascade decays.

The investigation of triple product correlations within SUSY at the LHC has been looked at for various different processes. Stop cascade decays were first studied in Ref. [23] and large CP-violating asymmetries were found. The study shown in Ref. [24] was the first to specifically examine stop decays in relation to the LHC and significant dilution factors were noted when parton distribution functions were introduced. Explicit dilution factors and initial estimates of the luminosity required at the LHC were shown for three-body decays in Ref. [25] and two-body decays in Ref. [17]. In addition $\tilde{t}_2$ decays were investigated in Ref. [26]. $\tilde{b}$ decays have also been looked at in similar studies for two-body cascade decays [27,28].

In Ref. [29] we looked at $\tilde{q}\,\tilde{g}$ production and decay and studied how to cope with statistical limitations and dilution factors in searching for CP phases in SUSY at the LHC. For the present paper, we extend the idea of momentum reconstruction, described in detail in Ref. [29] to $\tilde{t}$ production and two-body decays. We further include hadronic, combinatorial, and background effects to study whether CP violation will be observable in the $\tilde{t}$ sector at the LHC.

Regarding a precise measurement of ϕ_{A_t} at a future linear collider, we are not aware of any studies that measure CP violation in the stop sector directly. However, studies have been completed to measure the absolute value of A_t and are expected to be accurate to within 10% [30,31]. Also, there is the potential to study the CP properties of other third generation trilinear couplings, namely, those of the $\tilde{\tau}$ sector, ϕ_{A_τ} [32,33]. In addition, these studies may also be applicable to the LHC if tau polarization can be probed in the final state [34].

For our study, we consider the LHC production process,

$$pp \to \tilde{t}_1 \tilde{t}_1^*. \tag{2}$$

Our signal CP-odd observable is generated in the following two-body decays:

$$\tilde{t}_1 \to \tilde{\chi}_2^0 t, \qquad \tilde{\chi}_2^0 \to \tilde{\ell}\ell_N, \qquad \tilde{\ell} \to \tilde{\chi}_1^0 \ell_F, \qquad t \to bW, \tag{3}$$

where ℓ_N and ℓ_F denote the near and far leptons, respectively. The CP-odd observables are built from triple products of final-state momentum or reconstructable particles, e.g. $\vec{p}_{\ell_N} \cdot (\vec{p}_t \times \vec{p}_W)$.

Triple products constructed in this way are not Lorentz invariant but instead depend on the intrinsic boost of the produced particle in the laboratory frame. The observed asymmetry is maximal when the decay is at rest in the laboratory frame and any boost dilutes the observable. Consequently, we decided to use the idea of momentum reconstruction to find the momentum of the invisible $\tilde{\chi}_1^0$. We are able to perform momentum reconstruction for the decay chain shown in Eq. (3) as we have four on-shell mass conditions which we can solve for the four unknowns of the $\tilde{\chi}_1^0$ momentum on an event-by-event basis. Once the $\tilde{\chi}_1^0$ momentum is known, we can find the rest frame of any particle involved in the decay chain and thus measure the maximum CP asymmetry.

An important note to make is that the sign of the asymmetry generated by the triple product flips if we consider the decay of the charge conjugate $\tilde{t}_1^*$. Therefore, in addition to measuring the triple product we must also determine the charge of the decaying $\tilde{t}_1$. Unfortunately we cannot use a leptonically decaying W in this study as we must fully measure the t momentum to perform momentum reconstruction. Hence, we rely on the opposite $\tilde{t}_1$ decay to a single charged lepton final state to tag the charge of both produced stops, e.g. $\tilde{t}_1^* \to \tilde{\chi}_1^0 \bar{t}$, $\bar{t} \to \bar{b}\ell^- \bar{\nu}_\ell$. As an aside, charge identification of the process is also required to rule out T_N-odd observables that can in principle be generated by final-state interactions at the one-loop level [35]; see Sec. II B for more details. We compare the signal process with the charge-conjugated decay and, if a nonzero asymmetry is observed in the combination, it must correspond to a violation of CP symmetry.

Apart from backgrounds due to hard interactions, measuring asymmetries in a hadronic environment is challenging due to the high QCD activity and the underlying event that can be hard to disentangle from the signal process. However, the D0 Collaboration at the Tevatron has succeeded in making such a measurement with the like-sign dimuon charge asymmetry [36]. The asymmetry is interpreted to originate from the mixing of neutral B mesons and differs by 3.2 standard deviations from the standard model prediction. Therefore, the measurement is a significant hint of a new source of CP violation. Although this particular measurement is unlikely to be possible at the LHC due to the pp initial state, it does show that if the correct observables are chosen, asymmetry observations are possible at hadron colliders. In addition, the CDF Collaboration at the Tevatron has also recently made the observation of an asymmetry in the pair production of top quarks that also hints at new physics [37].

We begin in Sec. II by describing the process and underlying structure to derive the various triple products that can be formed. In Sec. III we discuss the momentum reconstruction method and its application to the process studied.

Section IV gives the analytical results of the asymmetries at parton level. Hadron level results are described in Sec. V, where we also discuss the effects of standard model and SUSY backgrounds. We also find that the method of momentum reconstruction significantly improves the signal-to-background ratio.

II. FORMALISM

A. The process studied and the amplitude squared

At the LHC, the light stop ($\tilde{t}_1$) particles can be produced via pair production,

$$pp \to \tilde{t}_1 \bar{\tilde{t}}_1^*, \tag{4}$$

which at the LHC will be dominated by the gluon fusion channels; see Fig. 1.

In our study the CP-violating observables are produced in the following decay:

$$\tilde{t}_1 \to \tilde{\chi}_2^0 t. \tag{5}$$

We require the $\tilde{\chi}_2^0$ to decay via two, two-body leptonic channels,

$$\tilde{\chi}_2^0 \to \tilde{\ell}_R^{\pm} \ell_N^{\mp} \to \tilde{\chi}_1^0 \ell_N^{\mp} \ell_F^{\pm}, \tag{6}$$

where N and F denote the near and far leptons, respectively. In addition, we only consider events where the t is fully reconstructable and hence decays hadronically,

$$t \to Wb \to q_u \bar{q}_d b. \tag{7}$$

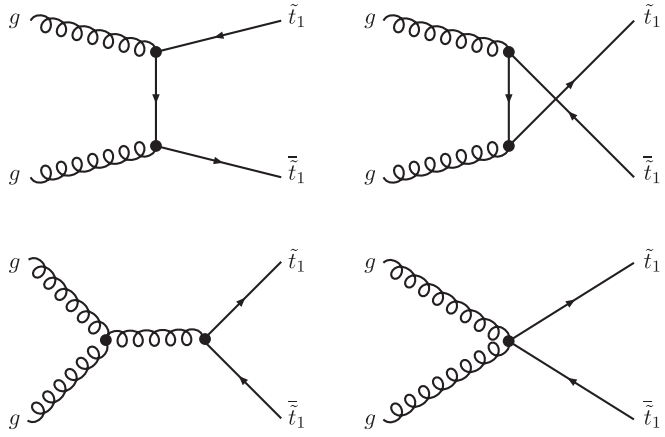

FIG. 1. Feynman diagrams for the production process $gg \to \tilde{t}_1 \bar{\tilde{t}}_1$.

Using the formalism of Refs. [38,39], the squared amplitude $|T|^2$ of the full process can be factorized into the processes of production $gg \to \tilde{t}_1 \bar{\tilde{t}}_1^*$ and the subsequent decays $\tilde{t}_1 \to t\tilde{\chi}_2^0$, $\tilde{\chi}_2^0 \to \tilde{\ell}\ell_N$, $\tilde{\ell} \to \tilde{\chi}_1^0 \ell_F$, and $t \to Wb$. We apply the narrow-width approximation but include the full spin correlations for the production and the decay of the intermediate particles, $\tilde{t}_1$, $\tilde{\chi}_2^0$, $\tilde{\ell}$, and t. The use of the narrow-width approximation is appropriate since the widths of the respective particles are much smaller than the masses in all cases. The squared amplitude can then be expressed in the form

$$|T|^2 = 4|\Delta(\tilde{t}_1)|^2 |\Delta(\tilde{\chi}_2^0)|^2 |\Delta(\tilde{\ell})|^2 |\Delta(t)|^2 P(\tilde{t}_1 \bar{\tilde{t}}_1^*) \{P(\tilde{\chi}_2^0 t) D(\tilde{\chi}_2^0) D(\tilde{\ell}) D(t) + \sum_{a=1}^{3} \Sigma_P^a(\tilde{\chi}_2^0) \Sigma_D^a(\tilde{\chi}_2^0) D(\tilde{\ell}) D(t)$$
$$+ \sum_{b=1}^{3} \Sigma_P^b(t) \Sigma_D^b(t) D(\tilde{\chi}_2^0) D(\tilde{\ell}) + \sum_{a,b=1}^{3} \Sigma_P^{ab}(\tilde{\chi}_2^0 t) \Sigma_D^a(\tilde{\chi}_2^0) \Sigma_D^b(t) D(\tilde{\ell})\}, \tag{8}$$

where $a, b = 1, 2, 3$ refer to the polarization states of the neutralino $\tilde{\chi}_i^0$ and top quark t. In addition,

(i) $\Delta(\tilde{t}_1)$, $\Delta(\tilde{\chi}_2^0)$, $\Delta(\tilde{\ell})$, and $\Delta(t)$ are the pseudopropagators of the intermediate particles which lead to the factors $E_{\tilde{t}_1}/m_{\tilde{t}_1}\Gamma_{\tilde{t}_1}$, $E_{\tilde{\chi}_2^0}/m_{\tilde{\chi}_2^0}\Gamma_{\tilde{\chi}_2^0}$, $E_{\tilde{\ell}_R}/m_{\tilde{\ell}_R}\Gamma_{\tilde{\ell}_R}$, and $E_t/m_t\Gamma_t$ in the narrow-width approximation.

(ii) $P(\tilde{t}_1\tilde{t}_1)$, $P(t\tilde{\chi}_2^0)$, $D(\tilde{\chi}_2^0)$, $D(\tilde{\ell})$, and $D(t)$ (Appendix D) are the terms in the production and decay that are independent of the spin of the decaying neutralino and top, whereas,

(iii) $\Sigma_P^a(\tilde{\chi}_i^0)$, $\Sigma_P^b(t)$, $\Sigma_P^{ab}(\tilde{\chi}_2^0 t)$, and $\Sigma_D^a(\tilde{\chi}_2^0)$, $\Sigma_D^b(t)$ (Appendix D) are the spin-dependent terms giving the correlations between production and decay of the $\tilde{\chi}_2^0$ and t. We follow the formalism and conventions described in Ref. [39].

(iv) It must be noted that the slepton $\tilde{\ell}$ produces no spin correlation term in the amplitude since it is a scalar.

Explicit expressions are given in Appendix D.

B. Structure of the T-odd asymmetry

As shown in the CPT-theorem [40,41], relativistic quantum field theories with usual spin-statistics relations have to be invariant under a CPT-transformation. This invariance guarantees that the masses and also the total widths of particles and antiparticles are the same. Since a true T-transformation is antiunitary, which exchanges the initial and the final states, it is useful to study naive T_N-transformations for collider-based experiments. The definition of T_N-transformations is to apply T-transformations to the initial and final states but without interchanging them. The unitarity of the S-matrix leads in the absence of rescattering effects (i.e., in leading order in perturbation theory, no final-state interactions and no width effects) to a conservation of the scattering amplitude under a CPT_N-transformation [35].

It is therefore useful to categorize CP-violating observables into T_N-odd and T_N-even observables. CPT_N

invariance implies that a T_N-odd observable is also CP-odd in the absence of rescattering effects. However, in case rescattering effects contribute, i.e. $CPT_N \neq CPT$-invariance, a T_N-odd signal may be caused by such rescattering effects and does not necessarily imply CP violation.

For all our observables we require that we know the charge of the decaying $\tilde{t}_1$ and can therefore distinguish the particle and antiparticle. Hence we can combine the process with the charge-conjugated decay to make an unambiguous observation of CP violation via T_N-odd observables.

In general, it is therefore important to classify all terms of the corresponding amplitude squared, Eq. (8), with respect to their T_N-odd or T_N-even character. Only the products that contain a T_N-odd contribution will lead to CP-odd violating observables:

(i) The spin-independent terms introduced in the previous section, $P(\tilde{t}_1\tilde{t}_1)$, $P(t\tilde{\chi}_2^0)$, $D(\tilde{\chi}_2^0)$, $D(\tilde{\ell})$, $D(t)$ do not cause any T_N-odd terms.

(ii) The spin-dependent terms, $\Sigma_P^a(\tilde{\chi}_i^0)$, $\Sigma_P^b(t)$, $\Sigma_P^{ab}(\tilde{\chi}_2^0 t)$, $\Sigma_D^a(\tilde{\chi}_2^0)$, $\Sigma_D^b(t)$, however, often can be divided up into T_N-even and T_N-odd terms, depending on the processes studied. In our case, a sequence of two-body decays, we can only split $\Sigma_P^{ab}(\tilde{\chi}_2^0 t) = \Sigma_{P,\text{even}}^{ab}(\tilde{\chi}_2^0 t) + \Sigma_{P,\text{odd}}^{ab}(\tilde{\chi}_2^0 t)$ and all other spin-dependent terms lead to T_N-even terms.[1]

(iii) Therefore, the T_N-odd term in the amplitude is $\sum_{a,b=1}^{3} \Sigma_{P,\text{odd}}^{ab}(\tilde{\chi}_2^0 t)\Sigma_D^a(\tilde{\chi}_2^0)\Sigma_D^b(t)D(\tilde{\ell})$.

When we contract the spin indices of the t and $\tilde{\chi}_2^0$ and evaluate the T_N-odd contribution, we find that the following covariant product appears in the amplitude:

$$\Sigma_{P,\text{odd}}^{ab}(\tilde{\chi}_2^0 t)\Sigma_D^a(\tilde{\chi}_2^0)\Sigma_D^b(t) \sim i\epsilon_{\mu\nu\rho\sigma} s^{a,\mu}(\tilde{\chi}_2^0) p^{\nu}_{\tilde{\chi}_2^0} s^{b,\rho}(t) p_t^{\sigma} \times (p_{\ell_N} s^a)(p_{[b,W]} s^b), \quad (9)$$

$$\sim i\epsilon_{\mu\nu\rho\sigma} p^{\nu}_{\tilde{\chi}_2^0} p^{\mu}_{\ell_N} p^{\rho}_W p_t^{\sigma}, \quad (10)$$

where $\Sigma_{P,\text{odd}}^{ab}$, $\Sigma_D^a(\tilde{\chi}_2^0)$, and $\Sigma_D^b(t)$ are given by Eqs. (D9), (D13), and (D15), respectively.

The above equation is multiplied by the imaginary part of the coupling, Eq. (D11), that contains terms from both the $\tilde{t}$, Eq. (A1), and $\tilde{\chi}^0$, Eq. (B1), mixing matrices. Hence, any complex phases contained in those mixing matrices will yield CP-violating effects that can be seen in an observable that exploits the covariant product. We can now expand the Lorentz invariant covariant product in terms of the explicit energy and momentum components,

$$\begin{aligned}\epsilon_{\mu\nu\rho\sigma} p^{\nu}_{\tilde{\chi}_2^0} p^{\mu}_{\ell_N} p^{\rho}_W p_t^{\sigma} &= E_{\tilde{\chi}_2^0}\vec{p}_{\ell_N} \cdot (\vec{p}_W \times \vec{p}_t) + E_W \vec{p}_t \cdot (\vec{p}_{\tilde{\chi}_2^0} \times \vec{p}_{\ell_N}) \\ &\quad - E_{\ell_N}\vec{p}_W \cdot (\vec{p}_t \times \vec{p}_{\tilde{\chi}_2^0}) - E_t \vec{p}_{\tilde{\chi}_2^0} \cdot (\vec{p}_{\ell_N} \times \vec{p}_W). \quad (11)\end{aligned}$$

The first term in Eq. (11) shows the CP-sensitive triple product that can be measured from final-state momenta. However, this triple product is not Lorentz invariant and consequently can vary in both magnitude and sign in different reference frames. If we are in the rest frame of the $\tilde{\chi}_2^0$ though,

$$\epsilon_{\mu\nu\rho\sigma} p^{\mu}_{\tilde{\chi}_2^0} p^{\nu}_{\ell_N} p^{\rho}_W p_t^{\sigma} \to m_{\tilde{\chi}_2^0}\vec{p}_{\ell_N} \cdot (\vec{p}_W \times \vec{p}_t), \quad (12)$$

the resulting asymmetry, Eq. (15), is uniquely defined since all other terms of the covariant product vanish as $\vec{p}_{\tilde{\chi}_2^0} \to 0$.

Hence we see that triple products of momenta can be used as T_N-odd observables. In this paper we find that the triple products most useful to study are

$$\mathcal{T}_{\ell_N} = \vec{p}_{\ell_N} \cdot (\vec{p}_W \times \vec{p}_t), \quad (13)$$

$$\mathcal{T}_{\ell\ell} = \vec{p}_b \cdot (\vec{p}_{\ell^+} \times \vec{p}_{\ell^-}), \quad (14)$$

where ℓ^+ and ℓ^- are the two leptons produced in the $\tilde{\chi}_2^0$ cascade decay. For the triple product, Eq. (14), the identification of near and far leptons is not required as is explained at the end of this section.

The T-odd asymmetry is then defined as

$$\mathcal{A}_T = \frac{N_{\mathcal{T}_+} - N_{\mathcal{T}_-}}{N_{\mathcal{T}_+} + N_{\mathcal{T}_-}} = \frac{\int \text{sign}\{\mathcal{T}_f\}|T|^2 d\,\text{lips}}{\int |T|^2 d\,\text{lips}}, \quad (15)$$

where $f = \ell_N$ or $\ell\ell$, $d$lips denotes Lorentz invariant phase space and $N_{\mathcal{T}_+}$ ($N_{\mathcal{T}_-}$) are the numbers of events for which $\mathcal{T}$ is positive (negative). The denominator in Eq. (15), $\int |T|^2 d\,\text{lips}$, is equal to the total cross section.

We then define

$$\mathcal{A}_{\ell_N} = \mathcal{A}_T(\mathcal{T}_{\ell_N}), \qquad \mathcal{A}_{\ell\ell} = \mathcal{A}_T(\mathcal{T}_{\ell\ell}), \quad (16)$$

where $\mathcal{A}_{\ell_N}$ is the asymmetry from the triple product $\mathcal{T}_{\ell_N}$ and $\mathcal{A}_{\ell\ell}$ is the asymmetry from the triple product $\mathcal{T}_{\ell\ell}$.

As stated above, while the covariant product is Lorentz invariant, the triple products are not. However, we can see that for the triple product in Eq. (13), the rest frame of the $\tilde{\chi}_2^0$ and the $\tilde{t}_1$ are equivalent since ($p_{\tilde{t}} = p_{\tilde{\chi}_2^0} + p_t$),

$$\epsilon_{\mu\nu\rho\sigma} p^{\mu}_{\tilde{\chi}_2^0} p^{\nu}_{\ell_N} p^{\rho}_W p_t^{\sigma} = \epsilon_{\mu\nu\rho\sigma} p^{\mu}_{\tilde{t}_1} p^{\nu}_{\ell_N} p^{\rho}_W p_t^{\sigma}. \quad (17)$$

For the triple product $\mathcal{T}_{\ell\ell}$, Eq. (14), the covariant product can be reexpressed in the following form (exploiting momentum conservation, $p_{\tilde{\chi}_2^0} = p_{\tilde{\ell}} + p_{\ell_N}$, $p_{\tilde{\ell}} = p_{\ell_F} + p_{\tilde{\chi}_1^0}$, $p_W = p_t + p_b$):

$$\epsilon_{\mu\nu\rho\sigma} p^{\mu}_{\tilde{\chi}_2^0} p^{\nu}_{\ell_N} p^{\rho}_W p_t^{\sigma} = \epsilon_{\mu\nu\rho\sigma}(p_{\ell_F} + p_{\tilde{\chi}_1^0})^{\mu} p^{\nu}_{\ell_N} p^{\rho}_W p_b^{\sigma}. \quad (18)$$

We now see that we have effectively two covariant products, one which contains the momentum of the $\tilde{\chi}_1^0$. In

[1]This is different if three-body decays are studied; see Ref. [25]. In that case spin-dependent terms from both the production $\Sigma_P^{ab}(\tilde{\chi}_2^0 t)$ as well as from the three-body decay $\Sigma_D^a(\tilde{\chi}_2^0)$ lead to CP-odd contributions.

general, triple products containing the momentum of the far lepton will be lower as the far lepton is not directly correlated with the spin of $\tilde{\chi}_2^0$. Nevertheless, we can exploit and maximize the triple products originating from Eq. (17) and (18), if we know the momentum of the unstable particles in the decay chain. This can be provided by the momentum reconstruction procedure described in the following section.

Changing the decaying $\tilde{t}_1$ to a $\tilde{t}_1^*$ or changing the charge of the near lepton ℓ_N reverses the sign of the covariant product. Consequently we have to know the charge of both the $\tilde{t}_1$ and the ℓ_N, otherwise any asymmetry will cancel. The charge of the $\tilde{t}_1$ can be found by demanding that the opposite cascade produces a single lepton and thus a trilepton final state. We distinguish the near and far leptons using the momentum reconstruction technique; see Sec. III. However if for some reason the leptons cannot be identified, we can still use the triple product $\mathcal{T}_{\ell\ell}$, Eq. (14). No lepton distinction is required as exchanging the near and far leptons has an extra sign change that cancels the change produced by the charge exchange.

III. MOMENTUM RECONSTRUCTION

A. Dilution effects

The triple product that is constructed from momenta in the laboratory frame suffers from dilution factors (~ 4) at the LHC. This is due to the lab frame being boosted with respect to the rest frame of the $\tilde{\chi}_2^0$ or $\tilde{t}_1$; see Eq. (17) and, for a more detailed discussion, Ref. [25]. It results in a considerable reduction in the maximum asymmetry observable when we introduce the parton distribution functions which causes an undetermined boost to the system. Figure 2 shows how the asymmetry is diluted in the laboratory frame when we produce the $\tilde{t}_1$ with varying initial momenta. If we were able to reconstruct the momentum of the $\tilde{t}_1$, we could perform a Lorentz transformation of all the momenta in the triple product into the $\tilde{t}_1$ rest frame and potentially recover the full asymmetry.

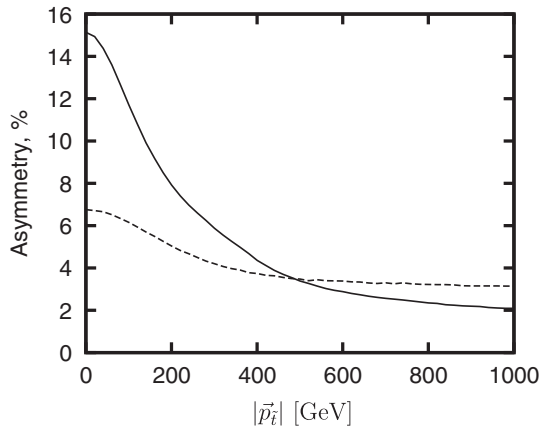

FIG. 2. The asymmetry $\mathcal{A}_T$, Eq. (15), as a function of the stop momentum, $|\vec{p}_{\tilde{t}}|$, in the laboratory frame. The solid line is the asymmetry for the triple product $\mathcal{T}_{\ell_N}$, Eq. (13), and the dotted line is for the triple product $\mathcal{T}_{\ell\ell}$, Eq. (14). The respective masses are given in Tables II, III, and IV.

B. Reconstruction procedure

We are able to reconstruct the $\tilde{\chi}_1^0$ four-momentum by reconstructing the following two-body decay chain in full (Fig. 3):

$$\tilde{t} \to t + \tilde{\chi}_2^0 \to t + \tilde{\ell}^{\pm} + \ell_N^{\mp} \to t + \tilde{\chi}_1^0 + \ell_N^{\mp} + \ell_F^{\pm}. \tag{19}$$

Assuming that all the masses in the decay chain are known, the kinematics can be fully reconstructed using the set of invariant mass conditions,

$$m^2_{\tilde{\chi}_1^0} = (p_{\tilde{\chi}_1^0})^2, \tag{20}$$

$$m^2_{\tilde{\ell}^{\pm}} = (p_{\tilde{\chi}_1^0} + p_{\ell_F^{\pm}})^2, \tag{21}$$

$$m^2_{\tilde{\chi}_2^0} = (p_{\tilde{\ell}^{\pm}} + p_{\ell_N^{\mp}})^2 = (p_{\tilde{\chi}_1^0} + p_{\ell_F^{\pm}} + p_{\ell_N^{\mp}})^2, \tag{22}$$

$$m^2_{\tilde{t}_1} = (p_{\tilde{\chi}_2^0} + p_t)^2 = (p_{\tilde{\chi}_1^0} + p_{\ell_F^{\pm}} + p_{\ell_N^{\mp}} + p_t)^2, \tag{23}$$

where p's denote the four-momenta of the respective particles.

We see that with the four equations we have enough information to solve the system and find each component of the $\tilde{\chi}_1^0$ four-momentum. A solution to the above set of equations is presented in Ref. [42] and we outline the procedure here. We first expand the $\tilde{\chi}_1^0$ momentum in terms of the final-state momentum of the $\ell_F^{\mp}$, $\ell_N^{\pm}$, and t,

$$\vec{p}_{\tilde{\chi}_1^0} = a\vec{p}_{\ell_F^{\pm}} + b\vec{p}_{\ell_N^{\mp}} + c\vec{p}_t. \tag{24}$$

In order to derive a system of three linear equations for the unknowns a–c, we calculate $\vec{p}_{\tilde{\chi}_1^0} \cdot \vec{p}_{\ell_F}$, $\vec{p}_{\tilde{\chi}_1^0} \cdot \vec{p}_{\ell_N}$, and $\vec{p}_{\tilde{\chi}_1^0} \cdot$

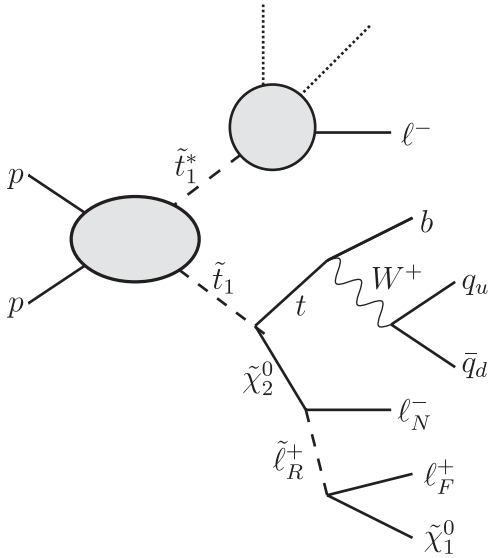

FIG. 3. The process studied for momentum reconstruction.

$\vec{p}_t$. Inserting Eq. (24) and exploiting Eqs. (21)–(23) we form the system of equations

$$\mathcal{M}\begin{pmatrix} a \\ b \\ c \end{pmatrix} = \begin{pmatrix} \frac{1}{2}(m^2_{\tilde{\chi}^0_1} - m^2_{\tilde{\ell}}) + E_{\tilde{\chi}^0_1} E_{\ell_F} \\ \frac{1}{2}(m^2_{\tilde{\ell}} - m^2_{\tilde{\chi}^0_2}) + p_{\ell_F} \cdot p_{\ell_N} + E_{\tilde{\chi}^0_1} E_{\ell_N} \\ \frac{1}{2}(m^2_{\tilde{\chi}^0_2} + m^2_t - m^2_{\tilde{t}_1}) + p_{\ell_F} \cdot p_t + p_{\ell_N} \cdot p_t + E_{\tilde{\chi}^0_1} E_t \end{pmatrix}, \tag{25}$$

where

$$\mathcal{M} = \begin{pmatrix} \vec{p}_{\ell_F} \cdot \vec{p}_{\ell_F} & \vec{p}_{\ell_F} \cdot \vec{p}_{\ell_N} & \vec{p}_{\ell_F} \cdot \vec{p}_t \\ \vec{p}_{\ell_N} \cdot \vec{p}_{\ell_F} & \vec{p}_{\ell_N} \cdot \vec{p}_{\ell_N} & \vec{p}_{\ell_N} \cdot \vec{p}_t \\ \vec{p}_t \cdot \vec{p}_{\ell_F} & \vec{p}_t \cdot \vec{p}_{\ell_N} & \vec{p}_t \cdot \vec{p}_t \end{pmatrix}. \tag{26}$$

We invert the matrix $\mathcal{M}$ to find solutions for a, b, and c in terms of constants and $E_{\tilde{\chi}^0_1}$. The on-shell mass condition for the $\tilde{\chi}^0_1$, Eq. (20), can then be expressed as

$$E^2_{\tilde{\chi}^0_1} = (a, b, c)\mathcal{M}\begin{pmatrix} a \\ b \\ c \end{pmatrix} + m^2_{\tilde{\chi}^0_1}. \tag{27}$$

We solve the above quadratic equation, to find two solutions for $E_{\tilde{\chi}^0_1}$. These solutions are then substituted back into Eq. (24) to find all components of the $\tilde{t}_1$ momentum on an event-by-event basis.

C. Challenges from multiple solutions

We encounter a complication in the reconstruction as Eq. (20) is quadratic in $p_{\tilde{\chi}^0_1}$. Consequently we have two solutions for $p_{\tilde{\chi}^0_1}$ for each reconstructed event but we have no extra information in the single decay chain to determine which solution is physically correct. As we cannot distinguish which of these solutions corresponds to the physically correct configuration, we need to analyze both. Therefore, we calculate the $\tilde{t}_1$ momentum for both configurations and boost all final-state particles in the triple product into the reconstructed $\tilde{t}_1$ rest frame. If the signs of both triple products are the same then the event is recorded but if the signs of the triple products are different, we discard the event since we cannot know which of the reconstructed solutions is correct. The method has the disadvantage that we lose events and therefore statistical significance. However, we find that the asymmetry can actually rise ($\approx 1.5\%$) as most of the events removed have small triple products and events with a small triple product lead to smaller asymmetries.

The procedure is essentially a cut designed for the triple product correlation observables. Events with an ambiguous triple product sign will significantly dilute the asymmetry and reduce the statistical significance of any CP-violating observation. Therefore, they must be removed from the sample. The disadvantage of the cut is that it makes an actual measurement of the CP-violating phase more involved. A comparison would have to be performed between a Monte Carlo simulation and the real data for a measurement to take place and may induce new errors. However, we believe that an actual determination of the phases at the LHC will be challenging and the method presented is more designed to establish the presence of CP violation in SUSY.

When performing the momentum reconstruction at the LHC we have additional problems from multiple solutions that come from combinatorial effects in the event. First, to complete the reconstruction we need to correctly identify the near and far lepton in the decay chain, Eq. (19), if we wish to compute the triple product $\mathcal{T}_{\ell_N}$, Eq. (13), although this information is not required for the triple product $\mathcal{T}_{\ell\ell}$, Eq. (14). We find that in $\approx 20\%$ of events the wrong assignment of near and far leptons satisfies the kinematic equations, Eqs. (20)–(23), and produces two extra solutions for the momentum of the $\tilde{\chi}^0_1$ in addition to the solutions found from the correct configuration. In addition, we always require a third lepton in the event coming from the opposite decay chain to correctly identify the stop charge. For example the lepton produced in the decay chain $\tilde{t}^*_1 \to \tilde{\chi}^- \bar{b}$, $\tilde{\chi}^- \to \ell^- + X$, where X are other neutral decay products. If this lepton is of the same flavor as those in the triple product decay chain there is a small chance that it can also reconstruct the $\tilde{\chi}^0_2$. All of these combinatorial issues are removed by again demanding that all calculated triple products are of the same sign and discarding any events where opposite sign solutions occur.

Further combinatorial issues occur with the reconstructed top in the event. First, a second b is always present in the opposite decay chain and this can occasionally combine with a reconstructed W to give a fake t. The opposite decay chain also can contain extra quarks that can produce more reconstructed t's. Finally, the parton shower can sometimes radiate hard gluons that are also seen as extra jets and further complicate the combinatorial problem. Whenever extra t quarks are found that satisfy the event kinematics, we perform the same procedure as for combinatorial leptons. Triple products are calculated for all reconstructed rest frames and only events that yield the same sign for all the reconstructed triple products are recorded.

D. Mass measurements

As mentioned above, we assume that the masses of all the SUSY particles in the decay chain will be known. However, for the majority of our equations in Eq. (25), we actually require the difference between various m^2's in the decay chains and not the absolute mass. At the LHC, the established way of measuring the SUSY spectrum is via mass end points (see Ref. [43] and references therein) and this method will measure these mass differences with high accuracy $\mathcal{O}(1\%)$.

The on-shell mass condition for the $\tilde{\chi}_1^0$ requires the absolute mass scale and this should be measured at the LHC to a precision of better than 10% [43], for low mass scenarios similar to the phenomenology presented in this paper. As an extra check on the numerical stability of the reconstruction procedure, up to 20 GeV absolute mass errors were tested on the absolute mass scale of the decay chain as a conservative estimate. This had a negligible effect on the reconstruction efficiency and the *CP* asymmetry and is therefore not considered to be a problem. In addition new methods have been proposed for measuring the sparticle masses from the kinematic invariants directly [42,44–48]. These methods also use the mass invariants on an event-by-event basis but use this information to reconstruct the masses of the particles in the decay chain. Therefore, these methods are directly measuring the inputs we require for Eqs. (20) and (25). We then use the output from these methods to reconstruct the momentum of the $\tilde{\chi}_1^0$ on an event-by-event basis. Reviews of all the major mass reconstruction methods proposed for the LHC are given in Refs. [49,50].

IV. PARTON LEVEL RESULTS

In this section we analyze numerically the *CP* asymmetry at the parton level, with the inclusion of parton distribution functions, while in Sec. V we complete a hadronic level study to estimate the effect in a realistic environment and the discovery potential at the LHC. In particular, we focus on a specific mSUGRA parameter point, Table I, at the parton level before discussing more general low mass mSUGRA scenarios for our hadronic study.

A. Chosen scenario: Spectrum and decay modes

We choose for this study the mSUGRA scenario shown in Table I with an added *CP* phase to the trilinear coupling ϕ_{A_t}. Although the value of the trilinear coupling is zero at the unification scale in this scenario, the renormalization group equations (RGEs) generate a value of $A_t = -391$ GeV at the weak scale. The spectrum at the electroweak scale has been derived using the RGE code SPHENO 2.2.3 [51] and the masses of the gauginos and scalars are shown in Tables II, III, and IV, respectively. Using the low energy soft SUSY-breaking parameters and the phase of the trilinear coupling ϕ_{A_t}, we calculate the masses and mixing of the $\tilde{t}_i$'s; see Appendix A for details.

For the presented analysis to work, we require the SUSY spectrum to have the following mass hierarchy:

$$m_{\tilde{t}_1} - m_t > m_{\tilde{\chi}_2^0} > m_{\tilde{\ell}_R^\pm} > m_{\tilde{\chi}_1^0}, \tag{28}$$

to allow for full momentum reconstruction. This hierarchy is often a feature in the mSUGRA parameter space. In addition we concentrate on scenarios with a light stop as the study is statistically limited and consequently we examine cases with a large production cross section.[2]

TABLE I. mSUGRA benchmark scenario (masses in GeV).

Parameter	m_0	$m_{1/2}$	$\tan\beta$	sign (μ)	A_0
Value	65	210	5	+	0

TABLE II. Masses (in GeV) of the gauginos calculated by SPHENO 2.2.3 [51].

Particle	$m_{\tilde{\chi}_1^0}$	$m_{\tilde{\chi}_2^0}$	$m_{\tilde{\chi}_3^0}$	$m_{\tilde{\chi}_4^0}$	$m_{\tilde{\chi}_1^\pm}$	$m_{\tilde{\chi}_2^\pm}$	$m_{\tilde{g}}$
Mass (GeV)	77.7	142.4	305.1	330.3	140.7	329.9	514.116

TABLE III. Masses (in GeV) of the squarks calculated by SPHENO 2.2.3 [51] except for the $\tilde{t}_i$ which were calculated at tree level for the phase $\phi_{A_t} = |\frac{4}{5}\pi|$.

Particle	$m_{\tilde{t}_1}$	$m_{\tilde{t}_2}$	$m_{\tilde{b}_1}$	$m_{\tilde{b}_2}$	$m_{\tilde{q}_{dL}}$	$m_{\tilde{q}_{dR}}$	$m_{\tilde{q}_{uL}}$	$m_{\tilde{q}_{uR}}$
Mass (GeV)	345.7	497.8	443.4	466.0	484.7	465.2	478.7	464.9

TABLE IV. Masses (in GeV) of the SUSY sleptons calculated by SPHENO 2.2.3 [51].

Particle	$m_{\tilde{\ell}_L}$	$m_{\tilde{\ell}_R}$	$m_{\tilde{\tau}_2}$	$m_{\tilde{\tau}_1}$
Mass (GeV)	163.4	110.8	164.9	108.0

The feasibility of the method at the LHC depends heavily on the integrated luminosity. For this reason we look closely at the predicted cross section of the asymmetry decay chain,

$$\sigma = \sigma(pp \to \tilde{t}_1\tilde{t}_1^*) \times BR(\tilde{t}_1 \to t\tilde{\chi}_2^0) \times BR(\tilde{\chi}_2^0 \to \tilde{\ell}^\pm \ell^\mp) \times BR(\tilde{\ell}^\pm \to \tilde{\chi}_1^0 \ell^\pm) \times BR(t \to q_u \bar{q}_d b), \tag{29}$$

and the relevant values for our scenario are shown in Table V. In our study we also need to identify the charge of the $\tilde{t}_1$ in the opposite decay chain and this is possible when the decay products contain a single lepton (any number of jets are allowed). We see that the dominant production of single leptons from $\tilde{t}_1$ decays is via the channel $\tilde{t}_1 \to \tilde{\chi}_1^+ b$. However, as only the right sleptons and the binolike $\tilde{\chi}_1^0$ are lighter than the winolike $\tilde{\chi}_1^+$, the decay of the $\tilde{\chi}_1^+$ is via mixing terms or Yukawa couplings and hence the decay $BR(\tilde{\chi}_1^+ \to \tilde{\tau}_1^+ \nu_\tau)$ dominates; see Table V. For this reason we find that our study is far more promising if τ identification is possible. We compare

[2]Since this paper was submitted, the particular parameter point, Table I, has been excluded [52,53]. However, the exclusion is derived from the gluino, first and second generation squark masses but the stop masses have far weaker bounds [54]. Therefore, if we do not restrict ourselves to a mSUGRA parameter space, the study is still valid.

TABLE V. Nominal values of the branching ratios (in %) for various decays calculated in HERWIG++ [55,56] with phase $\phi_{A_t} = |\frac{4}{5}\pi|$. In the last row, the calculated cross section for stop pair production at the LHC with $\sqrt{s} = 14$ TeV at leading order from HERWIG++.

Parameter	Value
$BR(\tilde{t}_1 \to \tilde{\chi}_1^0 t)$	34.6
$BR(\tilde{t}_1 \to \tilde{\chi}_2^0 t)$	7.5
$BR(\tilde{t}_1 \to \tilde{\chi}_1^+ b)$	50.1
$BR(\tilde{t}_1 \to \tilde{\chi}_2^+ b)$	7.8
$BR(\tilde{\chi}_2^0 \to \tilde{\mu}_R^+ \mu^-/\tilde{e}_R^+ e^-)$	11.6
$BR(\tilde{\chi}_1^+ \to \tilde{\tau}_1^+ \nu_\tau)$	95.1
$\sigma(pp \to \tilde{t}_1 \tilde{t}_1^*)$ [pb]	3.44

results where τ identification (with a 40% efficiency in the hadronic channels) has and has not been used in Sec. V.

B. *CP* asymmetry at the parton level

We start by discussing the dependence of the parton level asymmetry on ϕ_{A_t}, Eq. (15), for both the triple products $\mathcal{T}_{\ell_N}$ and $\mathcal{T}_{\ell\ell}$, Eqs. (13) and (14). In order to see the maximum dependence upon ϕ_{A_t}, we reconstruct the $\tilde{t}_1$ at rest and calculate the triple product in this frame. It should be noted that the asymmetry is obviously a *CP*-odd quantity; see Fig. 4.

We see from Fig. 4(a) that the largest asymmetry occurs for the triple product $\mathcal{T}_{\ell_N}$, which attains $|\mathcal{A}_{\ell_N}|_{\max} \approx 15\%$ when $\phi_{A_t} \approx 0.8\pi$. For the triple product $\mathcal{T}_{\ell\ell}$, the asymmetry is smaller, $|\mathcal{A}_{\ell\ell}|_{\max} \approx 6.5\%$, because the "true" *CP* triple product correlation is only partially measured; see Sec. II B.

If we now include the dominant production process at the LHC ($gg \to \tilde{t}_1 \bar{\tilde{t}}_1$) and relevant parton distribution functions (MRST 2004LO [57]), we see that the asymmetries are significantly diluted; see Fig. 4(b). The asymmetry for the triple product $\mathcal{T}_{\ell_N}$ drops from $|\mathcal{A}_{\ell_N}|_{\max} \approx 15\%$ to $|\mathcal{A}_{\ell_N}|_{\max} \approx 4.5\%$ and the reduction is due to the boosted frame of the produced $\tilde{t}_1$ as discussed in Sec. II B. For the triple product $\mathcal{T}_{\ell\ell}$, the reduction in the asymmetry is far less, from $|\mathcal{A}_{\ell\ell}|_{\max} \approx 6.5\%$ to $|\mathcal{A}_{\ell\ell}|_{\max} \approx 3.8\%$. This is because the triple product relies on the ℓ_F being correlated with the $\tilde{\ell}$ by the intrinsic boost of the $\tilde{\chi}_2^0$, $\tilde{\ell}$ system which already has a boost, even when the $\tilde{t}_1$ is at rest. As the $\tilde{t}_1$ becomes boosted, the boost of the $\tilde{\chi}_2^0$, $\tilde{\ell}$ system becomes proportionally less so, as the momentum of the $\tilde{t}_1$ is distributed throughout the decay chain. The difference in the dilution of the two asymmetries with $\tilde{t}$ momentum can be seen in Fig. 2.

V. HADRON LEVEL RESULTS

In order to estimate the potential for observing *CP*-violating effects in $\tilde{t}_1$ decays at the LHC more realistically, we perform the analysis at the hadronic level. We use the HERWIG++ [55,56] event generator to calculate all the matrix elements in the process, the initial hard interaction, the subsequent SUSY particle decays, the parton shower, and the hadronization. An important feature of HERWIG++ is that it calculates the spin correlations [58] in the SUSY cascade decay and allows the input of complex mixing matrices. Consequently, the triple product *CP* asymmetry can be automatically calculated within HERWIG++.

We also include both standard model and SUSY backgrounds in the analysis to understand how well $\tilde{t}_1 \tilde{t}_1^*$ production can be isolated at the LHC. We find that after applying basic signal identification cuts and the more complicated momentum reconstruction, virtually no standard model background contributes; see Sec. V B. However, the SUSY background presents more of a challenge and new cuts have to be introduced to improve the signal-to-background ratio (Sec. V D). Even after cuts, the

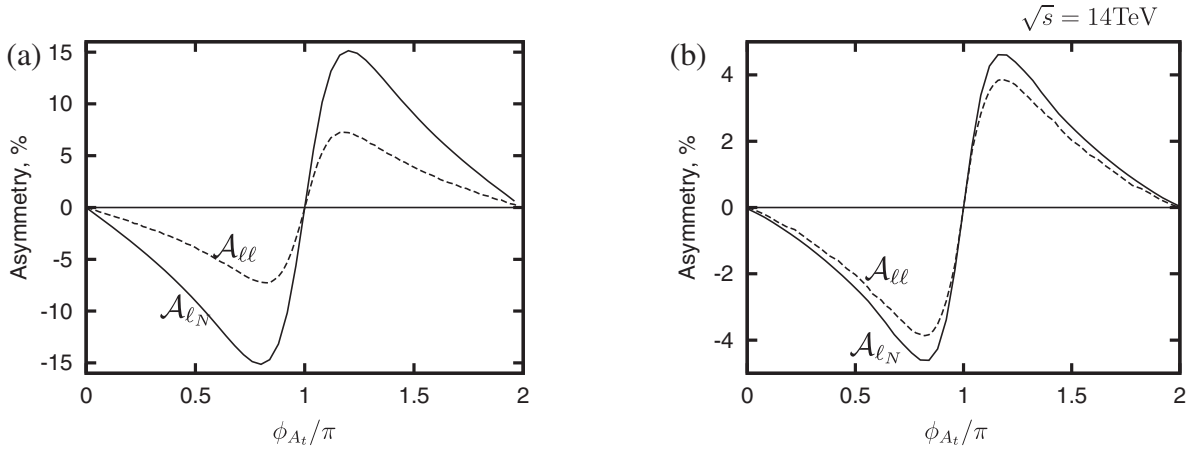

FIG. 4. (a) The asymmetry $\mathcal{A}_T$, Eq. (15), in the rest frame of $\tilde{t}_1$ as a function of ϕ_{A_t}. (b) The asymmetry $\mathcal{A}_T$, Eq. (15), in the laboratory frame as a function of ϕ_{A_t} at the LHC at 14 TeV. The solid line is the asymmetry for the triple product $\mathcal{T}_{\ell_N}$, Eq. (13), and the dotted line is for the triple product $\mathcal{T}_{\ell\ell}$, Eq. (14).

SUSY background can remain problematic but if the dominant contributions are known, the backgrounds can be partially subtracted.

A. Cuts used and signal identification

The hadronic analysis of the produced events has been performed within the program RIVET [59,60]. We used the anti-k_t [61,62] jet algorithm with $R = 0.5$ and applied the following acceptance cuts:

(i) $p_{T\ell_i} > 10$ GeV,
(ii) $p_{Tj_i} > 20$ GeV,
(iii) invariant mass of opposite sign same flavor (OSSF) leptons: $M_{\ell^+\ell^-} > 10$ GeV,
(iv) $|\eta_{\ell_i}| < 2.5$,
(v) $|\eta_{j_i}| < 3.5$,
(vi) lepton jet isolation, $\Delta R = 0.5$,
(vii) b-tag efficiency $= 60\%$ [63],
(viii) hadronic τ-tag efficiency $= 40\%$ [63] (whenever used).

To identify the events we demand three charged leptons in the final state, so that we can correctly identify the charge of each $\tilde{t}_1$ produced in the event; cf. Sec. II B. In addition, we demand that a pair of these leptons are OSSF as is the case for light leptons from $\tilde{\chi}_2^0$ decay. Whenever a $\tilde{t}_1$ decays in our scenarios a b is produced and therefore we require at least one b-tag in the final state (in principle we could require two b-tags including the opposite decay chain but we lose 40% of events due to b-tagging efficiency). On top of the b we require at least two more jets to be found in the final state so the full reconstruction of the t is possible. As all of our triple products and reconstructed momenta need a t, we require at least one hadronic t to be reconstructed. For this procedure, we first demand that two jets (not b's) reconstruct a $W^\pm$ ($70\ \text{GeV} < M_{jj} < 90\ \text{GeV}$). We then impose that a reconstructed $W^\pm$ and one b jet reconstruct a t ($150\ \text{GeV} < M_{W^\pm b} < 190\ \text{GeV}$).

Once these cuts have been passed we then perform the kinematical reconstruction shown in Sec. III with any t's and OSSF leptons found in the final state. If the particles satisfy the kinematic constraints, Eqs. (20)–(23), we will have at least two different solutions on an event-by-event basis for the momentum of the $\tilde{\chi}_1^0$. For each solution, the relevant rest frame triple product is calculated and only if all the signs of the triple products agree then the event is accepted.

B. Standard model background

The following standard model backgrounds were produced with HERWIG++: $t\bar{t}$, Drell-Yan (via γ and Z), W + jet, Z + jet, WW, WZ, ZZ, and $W\gamma$. In addition, we generate $t\bar{t}\ell^+\ell^-$ events with MADGRAPH [64] and then use HERWIG++ to perform the parton shower and hadronization. We find that after we produce an equivalent luminosity of 500 fb^{-1}, the only background to pass the event selection is $t\bar{t}\ell^+\ell^-$ with the very low rate of 0.03 events/fb^{-1} after kinematical reconstruction. This corresponds to only $\approx 1\%$ of the signal process for our particular scenario.

Although the above result is encouraging, it must be stated that our analysis contains no jets misidentified as leptons. As the dominant standard model contributions produced by HERWIG++ only contain two hard leptons in the initial process, the lack of a trilepton signal is not surprising. However, we do not expect major problems from standard model backgrounds if we limit the study to leptons from the first and second generation. $t\bar{t}$ can be expected to provide the largest background when both $W^\pm$ decay leptonically and an extra lepton is produced from a b or a misidentified jet. Even when this occurs though, we still require two additional hard jets in the event that have to combine with a b to form a t. Moreover, the final state then has to fulfill the reconstructed particular kinematics of our signal and finally all the calculated triple products have to agree.

To improve the statistical significance of our analysis, we also investigated the possibility of using τ-tagging in the opposite decay chain to that of our signal. In this analysis, we now change the original trilepton signal to a first or second lepton OSSF and additional hadronic τ. The misidentification of a jet for a τ is much higher than for the other leptons and the standard model backgrounds may now become an issue [63]. However, this analysis is postponed to future studies.

C. Stop production

We begin by studying $\tilde{t}_1\tilde{t}_1^*$ production along with the following decay chain:

$$\tilde{t}_1 \to \tilde{\chi}_2^0 t \to \tilde{\chi}_1^0 e^+ e^- j_u j_{\bar{d}} b, \tag{30}$$

$$\tilde{t}_1^* \to \tilde{\chi}_1^0 \bar{t} \to \tilde{\chi}_1^0 \mu^- \bar{\nu} b, \tag{31}$$

to test the momentum reconstruction procedure. The above decay chain is the cleanest signal process from a combinatorial point of view. We find a reconstruction efficiency of $\approx 5\%$ for this particular topology after cuts and the requirement for same sign triple products. The decay chain, Eq. (31), has a single lepton in the final state allowing us to tag the charge of both the $\tilde{t}_1$ and $\tilde{t}_1^*$ in the process.

For the CP asymmetry, we now concentrate purely on the triple product $\mathcal{T}_{\ell_N}$, Eq. (13), calculated in the reconstructed rest frame of the $\tilde{t}_1$, as this is the observable with high significance at the LHC. Figure 5(a) shows that there is virtually no dilution when we move to the hadronic level and the maximal asymmetry stays at $|\mathcal{A}_{\ell_N}|_{\max} \approx 15\%$. In fact, the hadronic level reconstruction does induce a degree of dilution, $\approx 1.5\%$, but this is canceled by our procedure of removing opposite sign triple products which enhances the asymmetry by a similar amount; cf. Sec. III C.

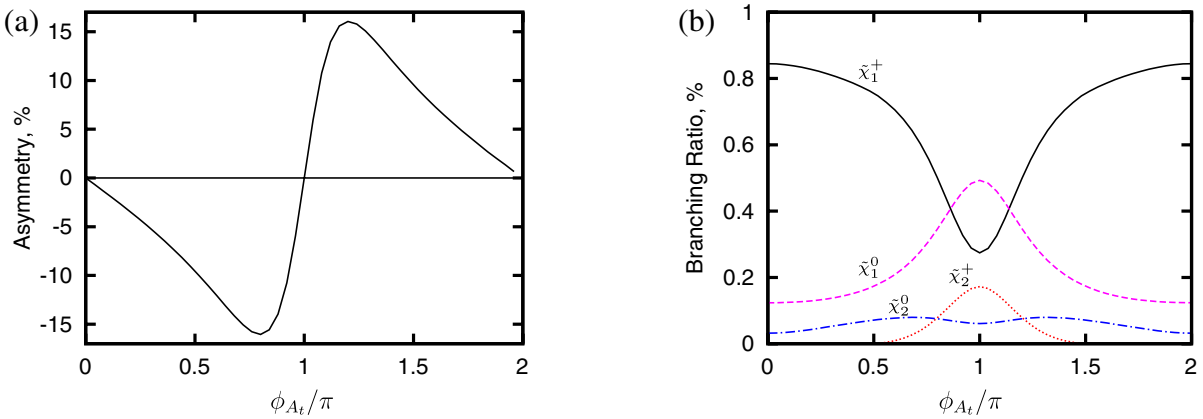

FIG. 5 (color online). (a) The asymmetry $\mathcal{A}_{\ell_N}$, Eq. (15), for the decay chain shown in Eqs. (30) and (31) as a function of ϕ_{A_t} at the hadronic level after momentum reconstruction has been performed. (b) The branching ratios: $\tilde{t}_1 \to \tilde{\chi}_1^+ b$ (black solid line), $\tilde{t}_1 \to \tilde{\chi}_2^+ b$ (red dotted line), $\tilde{t}_1 \to \tilde{\chi}_1^0 t$ (purple dashed line), and $\tilde{t}_1 \to \tilde{\chi}_2^0 t$ (blue dash-dotted line).

In order to estimate whether it is possible to observe a CP asymmetry in $\tilde{t}_1$ decays at the LHC, we need to calculate the statistical significance of any result. We assume that $N_{\mathcal{T}_+}(N_{\mathcal{T}_-})$, the numbers of events where $\mathcal{T}$ is positive (negative) as in Eq. (15), are binomially distributed, giving the following statistical error [65]:

$$\Delta(\mathcal{A}_T)^{\text{stat}} = 2\sqrt{\epsilon(1-\epsilon)/N}, \tag{32}$$

where $\epsilon = N_{\mathcal{T}_+}/(N_{\mathcal{T}_+} + N_{\mathcal{T}_-}) = \frac{1}{2}(1 + \mathcal{A}_T)$ and $N = N_{\mathcal{T}_+} + N_{\mathcal{T}_-}$ is the total number of events. Equation (32) can be rearranged to give the required number of events for a desired significance.

The total cross section used to calculate the statistical significance of any result in this paper has been calculated using HERWIG++ at the leading order (LO) for consistency. However, next-to-leading order (NLO) production cross sections are available and have been calculated using PROSPINO [66–68]; cf. Table VI. We see that in general the cross sections at NLO are higher than those at LO suggesting that the effective luminosity at the LHC will be more optimistic than that shown in the following results. In addition, the factorization and renormalization scale uncertainties are shown that indicate an estimate of the underlying theoretical uncertainty.

TABLE VI. Cross section at the LHC with $\sqrt{s} = 14$ TeV production channel $\tilde{t}_1\tilde{t}_1^*$ and colored SUSY production for both leading order and next-to-leading order. All cross sections were calculated using HERWIG++ [55,56] or PROSPINO [66–68]. The errors indicated next to the PROSPINO cross sections relate to varying the factorization and renormalization scales from $0.5m_{\tilde{t}_1} \to 2m_{\tilde{t}_1}$.

	$\tilde{t}_1\tilde{t}_1^*$	$\tilde{g}$, $\tilde{q}$
HERWIG++ LO [pb]	3.44	75.8
PROSPINO LO [pb]	$3.34^{+1.15}_{-0.8}$	$76.7^{+24.8}_{-17.3}$
PROSPINO NLO [pb]	$5.04^{+1.19}_{-0.92}$	$99.5^{+7.7}_{-9.6}$

Because of the phase dependence of both the $\tilde{t}_1$ branching ratios [see Fig. 5(b)] and production cross section, the statistical significance for different values of ϕ_{A_t} cannot be trivially extrapolated. The total number of events observed will be an interplay between the branching ratios and the production cross section. However, in the case of branching ratios, each of the decays, $\tilde{t}_1 \to \tilde{\chi}_1^+ b$, $\tilde{t}_1 \to \tilde{\chi}_2^+ b$, and $\tilde{t}_1 \to \tilde{\chi}_1^0 t$ has a different reconstruction efficiency and asymmetry dilution that needs to be calculated. For example, we see from Fig. 5(b) that the branching ratio for the decay $\tilde{t}_1 \to \tilde{\chi}_2^+ b$ increases noticeably as we vary ϕ_{A_t} from $\phi_{A_t} = 0$ to $\phi_{A_t} = |\pi|$ due to this decay becoming kinematically more favorable. The $\tilde{\chi}_2^+$ has a large number of final states with no lepton, however, so consequently the number of signal events decreases. Also, the $\tilde{\chi}_2^+$ decays generally contain extra jets that make the reconstruction of the event more difficult and thus reduce the efficiency of this channel.

Figure 6(a) shows the asymmetry when all $\tilde{t}_1$ decay channels are considered and an estimate of the amount of luminosity required for a 3σ-observation (statistical errors only) of a nonzero asymmetry for pure $\tilde{t}_1\tilde{t}_1^*$ production at the LHC. We can see that the asymmetry is slightly diluted when all $\tilde{t}_1$ decay modes are included from $|\mathcal{A}_{\ell_N}|_{\max} \approx 15\%$ to $|\mathcal{A}_{\ell_N}|_{\max} \approx 12.5\%$. The dilution is due to reconstructed events that are not originating from the signal process, Eq. (19). These events have no overall asymmetry and therefore simply dilute the signal. The horizontal lines in the figure show the estimate of the required luminosity required to see a certain asymmetry; an asymmetry can be seen at the 3σ level, where the asymmetry curve in Fig. 6(a) lies outside the luminosity band. The luminosity bands are not flat because, as discussed before, both the branching ratios and production cross section of the $\tilde{t}_1$ vary with the phase ϕ_{A_t}. We can see that in our scenario for pure

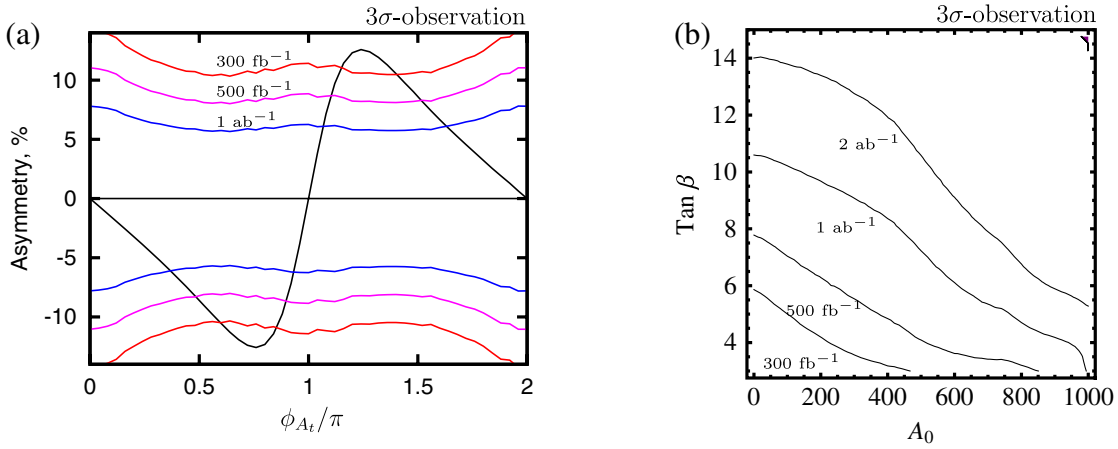

FIG. 6 (color online). Pure $\tilde{t}_1\tilde{t}_1^*$ production, all decay channels included; see Table V for branching ratios for the specific parameter point and Fig. 5 for how these alter with ϕ_{A_t}. τ-tagging is included in both plots. (a) Asymmetry, $\mathcal{A}_{\ell_N}$, at reference point with 3σ-luminosity lines shown. (b) Minimum luminosity required for 3σ-discovery in tanβ, A_0 plane (at the unification scale) when asymmetry, $\mathcal{A}_{\ell_N}$, is maximal.

$\tilde{t}_1\tilde{t}_1^*$ production, we expect a sensitivity for $0.5\pi < \phi_{A_t}(\mathrm{mod}\,\pi) < 0.9\pi$ with 500 fb^{-1}. With a combined analysis of both ATLAS and CMS data, this luminosity can be expected to be reached in the early 2020s if the LHC operates as is currently planned [69].

We can see the effect of varying the mSUGRA parameters tanβ and A_0 in Fig. 6(b). It is shown that, as the value of either tanβ or A_0 is increased, we require more luminosity to see a statistically significant observation even with maximum asymmetry. An increase in tanβ decreases the sensitivity because the branching ratio $\tilde{\chi}_2^0 \to \tilde{\ell}^{\pm}\ell^{\mp}$ is reduced. The reduction is due to $\tilde{\tau}$'s becoming more mixed which increases the left handed component in the lighter $\tilde{\tau}$. Therefore, the $\tilde{\tau}_1$ couples more strongly to the predominantly wino $\tilde{\chi}_2^0$ and begins to dominate this decay channel at the expense of the signal process. A rise in A_0 decreases sensitivity mainly because the CP asymmetry is reduced. The reason is that after RGE running, an increase in A_0 reduces the magnitude of the trilinear coupling A_t that contains the phase, ϕ_{A_t}, that we are interested in. Hence the CP effects are reduced.

Similarly, Fig. 7(a) shows the effect of varying the mSUGRA parameters m_0 and $m_{1/2}$ on the minimum luminosity required for an observation of CP effects. We note as general trend that, as $m_{1/2}$ is increasing, we need more luminosity to observe the CP-violating triple products. This is due to the increase in $\tilde{t}_1$ mass which reduces the production cross section for $\tilde{t}_1\tilde{t}_1^*$. If we increase m_0 we see that a large area of the parameter space has no two-body decay $\tilde{\chi}_2^0 \to \tilde{\ell}^{\pm}\ell^{\mp}$ as $m_{\tilde{\ell}^{\pm}} > m_{\tilde{\chi}_2^0}$.

Figure 7(b) indicates the effect of having no hadronic τ-tagging for the decay $\tilde{\chi}_1^+ \to \tilde{\tau}_1^+\nu_\tau$. The τ final state

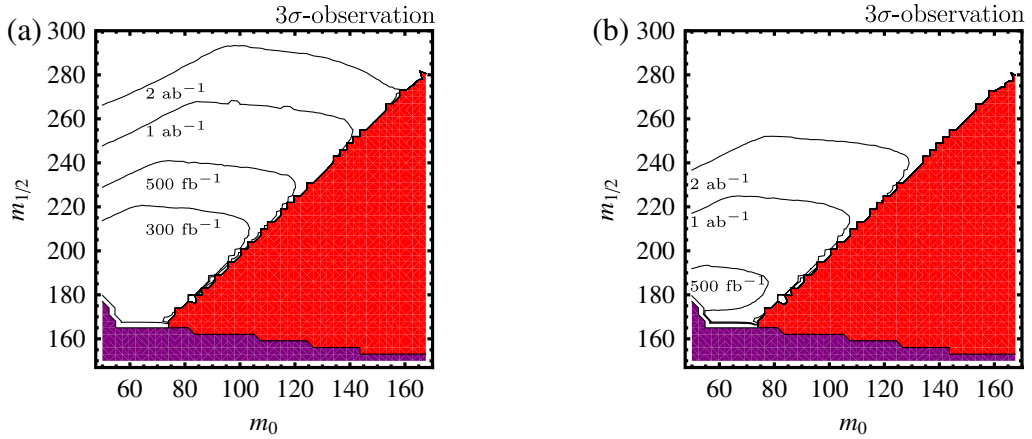

FIG. 7 (color online). Minimum luminosity required for 3σ-discovery in m_0, $m_{1/2}$ plane (at unification scale) when asymmetry, $\mathcal{A}_{\ell_N}$, is maximal. Pure $\tilde{t}_1\tilde{t}_1^*$ production, all decay channels included; see Table V for branching ratios for the specific parameter point and Fig. 5 for how these alter with ϕ_{A_t}. The lower purple area is ruled out by LEP direct detection [77] and the upper red area has no two-body decay $\tilde{\chi}_2^0 \to \tilde{\ell}^{\pm}\ell^{\mp}$. (a) With τ-tagging. (b) Without τ-tagging.

dominates the $\tilde{\chi}_1^+$ decay which in turn is the dominant product of the $\tilde{t}_1$ in low mass mSUGRA scenarios; see Table V. As stated in the beginning of Sec. V we assume a 40% τ-tagging efficiency and without this we lose approximately a factor of 2 in effective luminosity for our signal process.

D. Impact of momentum reconstruction on SUSY background separation

All of the previous section's results have assumed that the $\tilde{t}_1\tilde{t}_1^*$ process can be isolated effectively. However, in the mSUGRA scenarios investigated many other SUSY particles will be produced. Table VII shows that the total production cross section for SUSY is ≈ 25 times greater than for $\tilde{t}_1\tilde{t}_1^*$ production and we can therefore expect sizable backgrounds. We can also expect that the vast majority of the SUSY background processes will have no other spin correlated CP-sensitive triple product with the same final state and will therefore just act as a dilution to the CP asymmetry by contributing to the denominator of Eq. (15).

Table VII shows that after the initial event selection and top reconstruction, the SUSY background is still ≈ 10 times larger than the signal process. Note that if we apply the kinematical reconstruction to these events we see that we substantially reduce the background to be only ≈ 3 times larger.

In order to observe CP-violating effects in $\tilde{t}_1\tilde{t}_1^*$ production at the LHC, however, the signal-to-background ratio may still be too high and consequently we need further cuts to isolate the signal process. We notice that in mSUGRA scenarios, the largest background comes from $\tilde{g}$ production followed by the dominant decay to either sbottom, $\tilde{g} \rightarrow \tilde{b}_i b$ with a branching ratio of $\approx 30\%$. The $\tilde{b}_i$ decays dominantly to $\tilde{\chi}_2^0 b$ or $\tilde{\chi}_1^+ t$ which leads to a very similar final state as the signal process when combined with the opposite decay chain. The difference between the SUSY background and the $\tilde{t}_1$'s is that the $\tilde{g}$ and first and second generation $\tilde{q}$ have a higher mass. In addition, a gluino has in general one more decay vertex in the cascade decay producing another hard jet. These two factors mean that the average p_T of the particles produced in the event will be higher and the number of jets will be greater; thus we can use these characteristics to discriminate the signal from the background. Hence we cut on the number of jets reconstructed in an event,

$$\text{number of jets} < 6. \tag{33}$$

For the p_T cuts, we have

$$p_T(\text{hardest jet}) < 200\ \text{GeV}, \tag{34}$$

$$p_T(\text{2nd jet}) < 130\ \text{GeV}, \tag{35}$$

$$p_T(\text{3rd jet}) < 80\ \text{GeV (if applicable)}, \tag{36}$$

$$p_T(\text{any } b \text{ jet}) < 150\ \text{GeV}, \tag{37}$$

$$p_T(\text{any lepton}) < 100\ \text{GeV}. \tag{38}$$

Table VII shows that after all these cuts are performed the signal-to-background ratio improves significantly and we now have roughly the same number of signal and background events in the sample.

If we now reevaluate the luminosity plots with the SUSY background included, Figs. 8 and 9, we see that more luminosity is now required to observe a statistically significant effect. Because of the background dilution of the asymmetry, we now have $|\mathcal{A}_{\ell_N}|_{\max} \approx 6.5\%$ for our scenario; see Fig. 8. Consequently we are now only sensitive to phases between $0.6\pi < \phi_{A_t}(\text{mod}\pi) < 0.85\pi$ with 1 ab^{-1} of data. If we look at the tanβ, A_0 contour plot we see that sensitivity at the LHC for 1 ab^{-1} is only possible for small values of tanβ. A luminosity of 1 ab^{-1} would probably require an upgrade to the High-Luminosity LHC [70].

However, we would like to emphasize that it may be possible to substantially improve the statistical significance of an asymmetry measurement and return to close to the significance achieved when looking at a purely $\tilde{t}_1\tilde{t}_1^*$ process, even with the same SUSY background. Namely, via measuring the SUSY spectra (in particular the $\tilde{g}$ and $\tilde{b}$) a good estimate of the background should be possible. The background events can then be subtracted from the denominator of the asymmetry, Eq. (15), to give the true value of the asymmetry. Thus, the statistical significance should be much improved.

TABLE VII. Cross section, number of events, and signal-to-background ratio at the LHC with $\sqrt{s} = 14$ TeV at LO for both the production channel $\tilde{t}_1\tilde{t}_1^*$ and inclusive SUSY production. All cross sections were calculated using HERWIG++ [55,56].

	$\tilde{t}_1\tilde{t}_1^*$	SUSY	$\tilde{t}_1\tilde{t}_1^*$ Signal/SUSY background
Cross section [pb]	3.44	80.1	
Events with 500 fb^{-1}	1.7×10^6	4×10^7	
Events with 500 fb^{-1} initial selection	32 389	410 735	0.079
Events with 500 fb^{-1} top reconstruction	7117	64 729	0.11
Events with 500 fb^{-1} kinematic reconstruction	1213	3759	0.32
Events with 500 fb^{-1} extra SUSY cuts	901	967	0.93

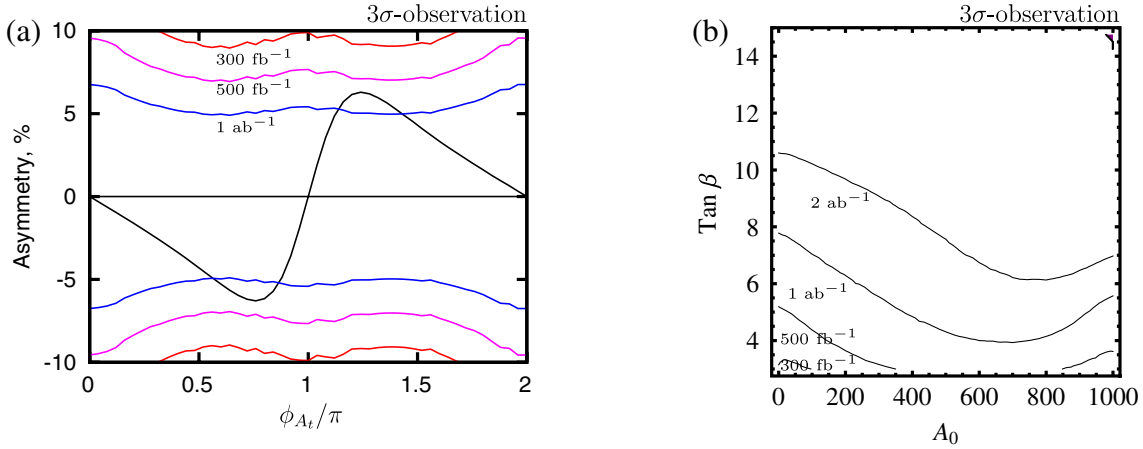

FIG. 8 (color online). General SUSY production for the asymmetry, $\mathcal{A}_{\ell_N}$. τ-tagging is included in both plots. (a) Asymmetry, $\mathcal{A}_{\ell_N}$, at reference point with 3σ-luminosity lines shown. (b) Minimum luminosity required for 3σ-discovery in tanβ, A_0 plane (at unification scale) when asymmetry, $\mathcal{A}_{\ell_N}$, is maximal.

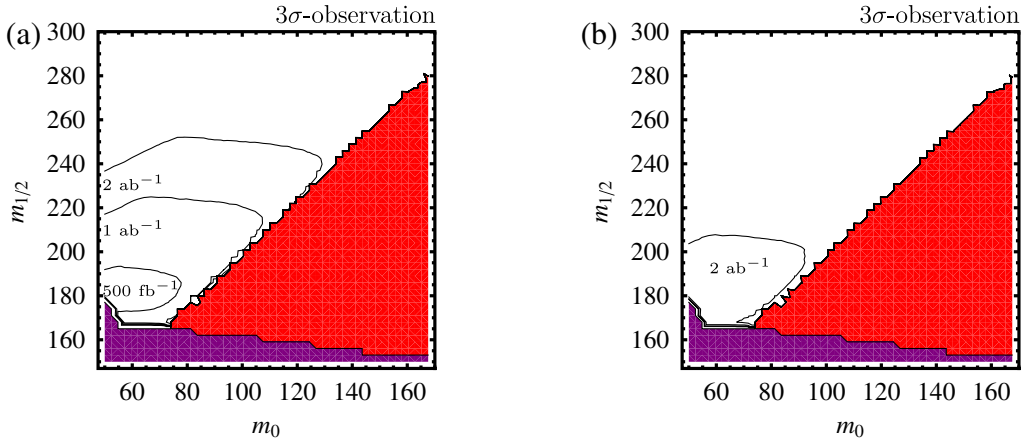

FIG. 9 (color online). General SUSY production for the asymmetry $\mathcal{A}_{\ell_N}$. Minimum luminosity required for 3σ-discovery in m_0, $m_{1/2}$ plane (at unification scale) when asymmetry, $\mathcal{A}_{\ell_N}$, is maximal. The lower purple area is ruled out by LEP direct detection [77] and the upper red area has no two-body decay $\tilde{\chi}_2^0 \to \tilde{\ell}^{\pm}\ell^{\mp}$. (a) With τ-tagging. (b) Without τ-tagging.

We would also like to remind the reader that this subtraction only becomes reliable if the signal-to-background ratio is good enough, otherwise the signal is swamped by statistical fluctuations. Thus the momentum reconstruction procedure is vital since it significantly reduces the backgrounds that are present.

Similarly, a more constrained area of observability is seen in the m_0, $m_{1/2}$ plane, Fig. 9(a). With 1 ab^{-1} of data, our study suggests that only if $m_{1/2} < 220$ GeV will it be possible to observe a CP phase in the stop sector. Again, we see the importance of τ-tagging to our study from the difference between Figs. 9(a) and 9(b). If τ-tagging is not used in the study, no CP violation in the $\tilde{t}_1$ sector can be observed with 1 ab^{-1} of data.

E. Open experimental issues

Although the presented study was completed at the hadronic level, a full detector simulation should be completed to confirm the conclusions of this paper. The most obvious experimental issue that could affect our results is the finite momentum resolution of the detector for both jets and leptons when performing momentum reconstruction. However, the resolution was tested with regards to momentum reconstruction in Ref. [29] with a significantly more complicated final state and it was found to have only a small effect.

In terms of background suppression the mistagging of various objects could increase both the standard model and SUSY background. For the standard model background, the most obvious example is the $t\bar{t}$ process generating a trilepton signal [63]. The process requires a jet to be mistagged as a lepton, which is not investigated in this study. The suitability of hadronic τ-tagging in the study also needs to be investigated thoroughly as these are expected to have significant misidentification rates [63]. However, this is beyond the scope of this theoretical study.

VI. CONCLUSIONS

In this paper we have investigated the problem of discovering *CP*-violating effects at the Large Hadron Collider. We studied $\tilde{t}_1\tilde{t}_1^*$ production and subsequent two-body decays. Triple product correlations can be formed from the final-state particles that are sensitive to the presence of complex phases in the model. Since triple products depend crucially on spin correlations and are therefore sensitive *CP*-odd observables, they have been included both in the analytical calculation and the event generation, that has been performed using HERWIG++. The process of special interest in our case was the $\tilde{t}_1$ decay into t and $\tilde{\chi}_2^0$ followed by two two-body leptonic decays. For this decay in our mSUGRA scenario one can expect an asymmetry in the triple product distribution of up to 15% when calculated in the rest frame of the decaying neutralino. The source of the *CP* violation in our case was the phase of the trilinear coupling A_t that attains a value of $\phi_{A_t} \sim 0.8$ when the asymmetry is maximum in our scenario.

Because of the hadronic experimental environment of the LHC, precise measurements will be a challenge both from experimental and theoretical point of view. The rest frame *CP*-odd asymmetry is diluted by the high boosts of the produced particles and this makes an observation difficult. We studied the impact of momentum reconstruction of invisible lightest supersymmetric particles to get access to the rest frame of the $\tilde{t}_1$. Using a set of invariant kinematic conditions we showed that it is possible to fully reconstruct the production and decay process on an event-by-event basis. The reconstruction was performed on events including the parton shower and hadronization. Having fully reconstructed events we are able to boost particle momenta back to the rest frame of the $\tilde{t}_1$ and the maximum asymmetry is recovered to 15%. In addition, momentum reconstruction leads to a significant increase in the signal-to-background ratio and thus is very important in attempting to isolate the process of interest.

If we consider exclusive $\tilde{t}_1$ production and all possible $\tilde{t}_1$ decay chains the maximum asymmetry is diluted slightly to $\sim$12.5%. In the mSUGRA scenario considered in this paper one should expect to see a 3σ effect at $\mathcal{L} = 500\ \mathrm{fb}^{-1}$ for phases in the range $0.5\pi \lesssim \phi_{A_t}(\mathrm{mod}\pi) \lesssim 0.9\pi$. If general SUSY production is considered, significant backgrounds to our signal process are present and extra kinematical cuts are required to remove this background. Even after these cuts some SUSY background remains and our maximum asymmetry is reduced to $\sim$6.5%. To see a 3σ effect at the LHC would require $\mathcal{L} = 1\mathrm{ab}^{-1}$ of data for sensitivity to phases in the range $0.6\pi \lesssim \phi_{A_t}(\mathrm{mod}\pi) \lesssim 0.85\pi$.

We emphasize that the asymmetry after momentum reconstruction is a much cleaner observable from a theoretical point of view, thanks to a well defined final state. Therefore, using the above technique provides prospects for the observation of *CP*-violating effects for a range of the phase ϕ_{A_t} after a few years of LHC running at the high luminosity. The full assessment of LHC's ability to resolve *CP* violation in the MSSM, however, will definitely require a detailed simulation of detector effects, SM, and SUSY backgrounds, which is beyond the scope of the present phenomenological analysis. The promising results of this study may encourage such further simulations.

ACKNOWLEDGMENTS

The authors wish to thank Peter Wienemann, Philip Bechtle, Björn Gosdzik, and Frank Krauss for valuable discussions. We also are grateful to David Grellscheid and Peter Richardson for their assistance in the use of HERWIG++. In addition we would like to thank Frank Siegert and Hendrik Hoeth for their help in the use of RIVET. K. R. was supported by the EU Network MRTN-CT-2006-035505 "Tools and Precision Calculations for Physics Discoveries at Colliders" (HEPTOOLS). J. T. was supported by the UK Science and Technology Facilities Council (STFC). The authors would like to thank the Helmholtz Alliance HA-101 "Physics at the Terascale" for support.

APPENDIX A: MIXING IN THE STOP SECTOR

In the minimal supersymmetric standard model the stop sector is defined by the mass matrix $\mathcal{M}_{\tilde{t}}$ in the basis of gauge eigenstates $(\tilde{t}_L, \tilde{t}_R)$. The 2×2 mass matrix depends on the soft scalar masses $M_{\tilde{Q}}$ and $M_{\tilde{U}}$, the supersymmetric Higgsino mass parameter μ, and the soft SUSY-breaking trilinear coupling A_t. It is given as [71]

$$\mathcal{M}_{\tilde{t}}^2 = \begin{pmatrix} m_t^2 + m_{LL}^2 & m_{LR}^* m_t \\ m_{LR} m_t & m_t^2 + m_{RR}^2 \end{pmatrix}, \tag{A1}$$

where

$$m_{LL}^2 = M_{\tilde{Q}}^2 + m_Z^2 \cos 2\beta \left(\frac{1}{2} - \frac{2}{3}\sin^2\theta_W\right), \tag{A2}$$

$$m_{RR}^2 = M_{\tilde{U}}^2 + \frac{2}{3} m_Z^2 \cos 2\beta \sin^2\theta_W, \tag{A3}$$

$$m_{LR} = A_t - \mu^* \cot\beta, \tag{A4}$$

and $\tan\beta = v_2/v_1$ is the ratio of the vacuum expectation values of the two neutral Higgs fields which break the electroweak symmetry. From the above parameters only μ and A_t can take complex values,

$$A_t = |A_t| e^{i\phi_{A_t}}, \quad \mu = |\mu| e^{i\phi_\mu}, \quad (0 \le \phi_{A_t}, \phi_\mu < 2\pi), \tag{A5}$$

thus yielding *CP* violation in the stop sector.

The Hermitian matrix $\mathcal{M}_{\tilde{t}}^2$ is diagonalized by a unitary matrix $\mathcal{R}_{\tilde{t}}$,

$$\mathcal{R}_{\tilde{t}} \mathcal{M}_{\tilde{t}}^2 \mathcal{R}_{\tilde{t}}^\dagger = \begin{pmatrix} m_{\tilde{t}_1}^2 & 0 \\ 0 & m_{\tilde{t}_2}^2 \end{pmatrix}, \tag{A6}$$

where we choose the convention $m^2_{\tilde{t}_1} < m^2_{\tilde{t}_2}$ for the masses of $\tilde{t}_1$ and $\tilde{t}_2$. The matrix $\mathcal{R}_{\tilde{t}}$ rotates the gauge eigenstates, $\tilde{t}_L$ and $\tilde{t}_R$, into the mass eigenstates $\tilde{t}_1$ and $\tilde{t}_2$ as follows:

$$\begin{pmatrix}\tilde{t}_1\\ \tilde{t}_2\end{pmatrix} = \mathcal{R}\begin{pmatrix}\tilde{t}_L\\ \tilde{t}_R\end{pmatrix} = \begin{pmatrix}\cos\theta_{\tilde{t}} & \sin\theta_{\tilde{t}} e^{-i\phi_{\tilde{t}}}\\ -\sin\theta_{\tilde{t}} e^{i\phi_{\tilde{t}}} & \cos\theta_{\tilde{t}}\end{pmatrix}\begin{pmatrix}\tilde{t}_L\\ \tilde{t}_R\end{pmatrix}, \tag{A7}$$

where $\theta_{\tilde{t}}$ and $\phi_{\tilde{t}}$ are the mixing angle and the CP-violating phase of the stop sector, respectively. The masses are given by

$$m_{\tilde{t}_{1,2}} = \frac{1}{2}(2m_t^2 + m_{LL}^2 + m_{RR}^2 \mp \sqrt{(m_{LL}^2 - m_{RR}^2)^2 + 4|m_{LR}|^2 m_t^2}), \tag{A8}$$

whereas for the mixing angle and the CP phase we have

$$\cos\theta_{\tilde{t}} = \frac{-m_t|m_{LR}|}{\sqrt{m_t^2|m_{LR}|^2 + (m^2_{\tilde{t}_1} - m_{LL}^2)^2}}, \tag{A9}$$

$$\sin\theta_{\tilde{t}} = \frac{m_{LL}^2 - m^2_{\tilde{t}_1}}{\sqrt{m_t^2|m_{LR}|^2 + (m^2_{\tilde{t}_1} - m_{LL}^2)^2}}, \tag{A10}$$

$$\phi_{\tilde{t}} = \arg(A_t - \mu^* \cot\beta). \tag{A11}$$

By convention we take $0 \le \theta_{\tilde{t}} < \pi$ and $0 \le \phi_{\tilde{t}} < 2\pi$. It must be noted that $\phi_{\tilde{t}}$ is an "effective" phase and does not directly correspond to the phase of any MSSM parameter. Instead, the phase will have contributions from both ϕ_{A_t} and ϕ_μ. However, in this study we set $\phi_\mu = 0$ due to the EDM constraints.

If $m_{LL} < m_{RR}$ then $\cos^2\theta_{\tilde{t}} > \frac{1}{2}$ and $\tilde{t}_1$ has a predominantly left gauge character. On the other hand, if $m_{LL} > m_{RR}$ then $\cos^2\theta_{\tilde{t}} < \frac{1}{2}$ and $\tilde{t}_1$ has a predominantly right gauge character.

APPENDIX B: MIXING IN THE NEUTRALINO SECTOR

In the MSSM, the four neutralinos $\tilde{\chi}_i^0$ $(i = 1, 2, 3, 4)$ are mixtures of the neutral $U(1)$ and $SU(2)$ gauginos, $\tilde{B}$ and $\tilde{W}^3$, and the Higgsinos, $\tilde{H}_1^0$ and $\tilde{H}_2^0$. The neutralino mass matrix in the $(\tilde{B}, \tilde{W}^3, \tilde{H}_1^0, \tilde{H}_2^0)$ basis [72,73]

$$\mathcal{M}_N = \begin{pmatrix} M_1 & 0 & -m_Z c_\beta s_W & m_Z s_\beta s_W \\ 0 & M_2 & m_Z c_\beta c_W & -m_Z s_\beta c_W \\ -m_Z c_\beta s_W & m_Z c_\beta c_W & 0 & -\mu \\ m_Z s_\beta s_W & -m_Z s_\beta c_W & -\mu & 0 \end{pmatrix} \tag{B1}$$

is built up by the fundamental SUSY parameters: the $U(1)$ and $SU(2)$ gaugino masses M_1 and M_2, the Higgsino mass parameter μ, and $\tan\beta = v_2/v_1$ ($c_\beta = \cos\beta$, $s_W = \sin\theta_W$, etc.). In addition to the μ parameter, a nontrivial CP phase can also be attributed to the M_1 parameter,

$$M_1 = |M_1| e^{i\phi_1}, \qquad (0 \le \phi_1 < 2\pi). \tag{B2}$$

Because the complex matrix $\mathcal{M}_N$ is symmetric, one unitary matrix N is sufficient to rotate the gauge eigenstate basis $(\tilde{B}, \tilde{W}^3, \tilde{H}_1^0, \tilde{H}_2^0)$ to the mass eigenstate basis of the Majorana fields $\tilde{\chi}_i^0$

$$\begin{aligned} &\mathrm{diag}\,(m_{\tilde{\chi}_1^0}, m_{\tilde{\chi}_2^0}, m_{\tilde{\chi}_3^0}, m_{\tilde{\chi}_4^0}) = N^* \mathcal{M}_N N^\dagger, \\ &(m_{\tilde{\chi}_1^0} < m_{\tilde{\chi}_2^0} < m_{\tilde{\chi}_3^0} < m_{\tilde{\chi}_4^0}). \end{aligned} \tag{B3}$$

The masses $m_{\tilde{\chi}_i^0}$ $(i = 1, 2, 3, 4)$ can be chosen to be real and positive by a suitable definition of the unitary matrix N.

APPENDIX C: INTERACTION LAGRANGIAN AND COUPLINGS

The interaction Lagrangian for the stop decay $(\tilde{t}_i \to \tilde{\chi}_j^0 t)$ is

$$\mathcal{L}_{t\tilde{t}\tilde{\chi}^0} = \tilde{\chi}_j^0 (a_{ij} P_L + b_{ij} P_R) t \tilde{t}_i^* + \text{H.c.}, \tag{C1}$$

where $P_{L,R} = \frac{1}{2}(1 \mp \gamma_5)$. The couplings are given by

$$a_{ij} = -\frac{e}{\sqrt{2} s_W c_W} \mathcal{R}^{\tilde{t}}_{i1} \left(\frac{1}{3} s_W N^*_{j1} + c_W N^*_{j2}\right) - Y_t \mathcal{R}^{\tilde{t}}_{i2} N^*_{j4}, \tag{C2}$$

$$b_{ij} = \frac{2\sqrt{2} e}{3 c_W} \mathcal{R}^{\tilde{t}}_{i2} N_{j1} - Y_t \mathcal{R}^{\tilde{t}}_{i1} N_{j4}, \tag{C3}$$

where $\mathcal{R}^{\tilde{t}}_{ij}$ are the entries of stop mixing matrix, Eq. (A7), and N_{ij} are the entries of the neutralino mixing matrix, Eq. (B3). The top Yukawa coupling is given by

$$Y_t = \frac{e m_t}{\sqrt{2} m_W s_W \sin\beta}. \tag{C4}$$

The interaction Lagrangian for the neutralino decay $(\tilde{\chi}_j^0 \to \tilde{\ell}\ell)$ is

$$\mathcal{L}_{\ell\tilde{\ell}\tilde{\chi}_j^0} = g f^\ell_{Lj} \bar{\ell} P_R \tilde{\chi}_j^0 \tilde{\ell}_L + g f^\ell_{Rj} \bar{\ell} P_L \tilde{\chi}_j^0 \tilde{\ell}_R + \text{H.c.}, \tag{C5}$$

where $g = e/\sin\theta_W$. The couplings are given by

$$f^\ell_{Lj} = \frac{1}{\sqrt{2}} (\tan\theta_W N_{j1} + N_{j2}), \tag{C6}$$

$$f^\ell_{Rj} = -\sqrt{2} \tan\theta_W N^*_{j1}. \tag{C7}$$

APPENDIX D: AMPLITUDE SQUARED INCLUDING FULL SPIN CORRELATIONS

1. Neutralino production $\tilde{t}_1 \to \tilde{\chi}_j^0 t$

Here we give the analytic expression for the neutralino production density matrix [23],

$$|M(\tilde{t}_1 \to \tilde{\chi}_j^0 t)|^2 = P(\tilde{\chi}_j^0 t) + \Sigma_P^a(\tilde{\chi}_j^0) + \Sigma_P^b(t) + \Sigma_P^{ab}(\tilde{\chi}_j^0 t), \tag{D1}$$

whose spin-independent contribution reads

$$P(\tilde{\chi}_j^0 t) = (|a_{1j}|^2 + |b_{1j}|^2)(p_t p_{\tilde{\chi}_j^0}) - 2 m_t m_{\tilde{\chi}_j^0} Re(a_{1j} b_{1j}^*), \tag{D2}$$

where p_t and $p_{\tilde{\chi}_k^0}$ denote the four-momenta of the t-quark and the neutralino $\tilde{\chi}_k^0$. The coupling constants a_{ij} and b_{ij} are shown in Eqs. (C2) and (C3), and by substituting the explicit matrix elements of Eq. (A7) we can show the specific parameter dependence [74],

$$|a_{1j}|^2 + |b_{1j}|^2 = \cos^2\theta_{\tilde{t}} \left(\frac{e^2}{2 s_W^2 c_W^2} |\frac{1}{3} s_W N_{j1} + c_W N_{j2}|^2 + Y_t^2 |N_{j4}|^2 \right) + \sin^2\theta_{\tilde{t}} \left(\frac{8 e^2}{9 c_W^2} |N_{j1}|^2 + Y_t^2 |N_{j4}|^2 \right)$$
$$+ 2 \sin\theta_{\tilde{t}} \cos\theta_{\tilde{t}} Y_t \left(\frac{e}{\sqrt{2} s_W c_W} \mathrm{Re}\left[e^{i\phi_{\tilde{t}}} \left(\frac{1}{3} s_W N_{j1}^* + c_W N_{j2}^* \right) N_{j4} \right] - \frac{2\sqrt{2} e}{3 c_W} \mathrm{Re}[e^{-i\phi_{\tilde{t}}} N_{j1} N_{j4}^*] \right), \tag{D3}$$

$$\mathrm{Re}[a_{1j} b_{1j}^*] = \cos^2\theta_{\tilde{t}} \frac{e}{\sqrt{2} s_W c_W} Y_t \mathrm{Re}\left[\left(\frac{1}{3} s_W N_{j1}^* + c_W N_{j2}^* \right) N_{j4}^* \right] + \sin^2\theta_{\tilde{t}} \frac{2\sqrt{2} e}{3 c_W} Y_t \mathrm{Re}[N_{j4}^* N_{j1}^*]$$
$$+ \sin\theta_{\tilde{t}} \cos\theta_{\tilde{t}} \left(Y_t^2 \mathrm{Re}[e^{-i\phi_{\tilde{t}}} N_{j4}^{*2}] - \frac{2}{3} \frac{e^2}{s_W c_W^2} \mathrm{Re}\left[e^{i\phi_{\tilde{t}}} \left(\frac{1}{3} s_W N_{j1}^* + c_W N_{j2}^* \right) N_{j1}^* \right] \right). \tag{D4}$$

The spin-dependent terms that depend on individual spin contributions are T-even and are given by

$$\Sigma_P^a(\tilde{\chi}_j^0) = (|b_{ij}|^2 - |a_{ij}|^2) m_{\tilde{\chi}_j^0} (p_t s^a(\tilde{\chi}_j^0)), \tag{D5}$$

$$\Sigma_P^b(t) = (|b_{ij}|^2 - |a_{ij}|^2) m_t (p_{\tilde{\chi}_j^0} s^b(t)), \tag{D6}$$

where $s^a(\tilde{\chi}_j^0)$ and $(s^b(t))$ denote the spin-basis vectors of the neutralino $\tilde{\chi}_j^0$ (t-quark). Again the coupling constants can be expanded as

$$|b_{1j}|^2 - |a_{1j}|^2 = \cos^2\theta_{\tilde{t}} \left(Y_t^2 |N_{j4}|^2 - \frac{e^2}{2 s_W^2 c_W^2} |\frac{1}{3} s_W N_{j1} + c_W N_{j2}|^2 \right) + \sin^2\theta_{\tilde{t}} \left(\frac{8 e^2}{9 c_W^2} |N_{j1}|^2 - Y_t^2 |N_{j4}|^2 \right)$$
$$- 2 \sin\theta_{\tilde{t}} \cos\theta_{\tilde{t}} Y_t \left(\frac{e}{\sqrt{2} s_W c_W} \mathrm{Re}\left[e^{i\phi_{\tilde{t}}} \left(\frac{1}{3} s_W N_{j1}^* + c_W N_{j2}^* \right) N_{j4} \right] + \frac{2\sqrt{2} e}{3 c_W} \mathrm{Re}[e^{-i\phi_{\tilde{t}}} N_{j1} N_{j4}^*] \right). \tag{D7}$$

The terms that depend simultaneously on the spin of the top quark and of the neutralino can be split into T-even, $\Sigma_{P,\mathrm{even}}^{ab}(\tilde{\chi}_j^0 t)$, and T-odd, $\Sigma_{P,\mathrm{odd}}^{ab}(\tilde{\chi}_j^0 t)$. The T-even contributions are as follows:

$$\Sigma_{P,\mathrm{even}}^{ab}(\tilde{\chi}_j^0 t) = 2\,\mathrm{Re}(a_{ij} b_{ij}^*)[(s^a(\tilde{\chi}_j^0) p_t)(s^b(t) p_{\tilde{\chi}_j^0}) - (p_t p_{\tilde{\chi}_j^0})(s^a(\tilde{\chi}_j^0) s^b(t))] + m_t m_{\tilde{\chi}_j^0} (s^a(\tilde{\chi}_j^0) s^b(t))(|a_{ij}|^2 + |b_{ij}|^2). \tag{D8}$$

The T-odd contributions that generate the triple product correlations that we are interested in are

$$\Sigma_{P,\mathrm{odd}}^{ab}(\tilde{\chi}_j^0 t) = -g^2\,\mathrm{Im}(a_{ij} b_{ij}^*) f_4^{ab}, \tag{D9}$$

where the T-odd kinematical factor is given by

$$f_4^{ab} = \epsilon_{\mu\nu\rho\sigma} s^{a,\mu}(\tilde{\chi}_j^0) p_{\tilde{\chi}_j^0}^\nu s^{b,\rho}(t) p_t^\sigma. \tag{D10}$$

Section II B explains how this epsilon product generates the triple product observable. We again expand the coupling constant to see the functional dependence,

$$\mathrm{Im}[a_{1j}b_{1j}^*] = \cos^2\theta_{\tilde{t}}\frac{e}{\sqrt{2}s_W c_W}Y_t\,\mathrm{Im}\left[\left(\frac{1}{3}s_W N_{j1}^* + c_W N_{j2}^*\right)N_{j4}^*\right] + \sin^2\theta_{\tilde{t}}\frac{2\sqrt{2}e}{3c_W}Y_t\,\mathrm{Im}[N_{j4}^* N_{j1}^*]$$
$$+ \sin\theta_{\tilde{t}}\cos\theta_{\tilde{t}}(Y_t^2\,\mathrm{Im}[e^{-i\phi_{\tilde{t}}}N_{j4}^{*2}] - \frac{2}{3}\frac{e^2}{s_W c_W^2}\,\mathrm{Im}\left[e^{i\phi_{\tilde{t}}}\left(\frac{1}{3}s_W N_{j1}^* + c_W N_{j2}^*\right)N_{j1}^*\right]). \quad \text{(D11)}$$

2. Neutralino decay $\tilde{\chi}_2^0 \to \tilde{\ell}_R^+\ell^-$

We provide analytical expressions for the two-body decay of the $\tilde{\chi}_2^0$ into a $\tilde{\ell}_R^+$ and the final-state ℓ^- [75],

$$D(\tilde{\chi}_2^0) = \frac{g^2}{4}|f_{L2}^l|^2\{m_{\tilde{\chi}_2^0}^2 - m_{\tilde{\ell}_R}^2\}. \quad \text{(D12)}$$

The spin-dependent contribution is T-even and reads

$$\Sigma_D^a(\tilde{\chi}_2^0) = \frac{g^2}{2}|f_{L2}^l|^2 m_{\tilde{\chi}_2^0}(s^a(\tilde{\chi}_2^0)p_{\ell^-}). \quad \text{(D13)}$$

3. Top decay $t \to W^+ b$

We provide analytical expressions for the two-body decay of the top quark into a W-boson and the final-state bottom quark [76],

$$D(t) = \frac{g^2}{4}\left\{m_t^2 - 2m_W^2 + \frac{m_t^4}{m_W^2}\right\}. \quad \text{(D14)}$$

The spin-dependent contribution is T-even and reads

$$\Sigma_D^b(t) = -\frac{g^2}{2}m_t\left\{(s^b(t)p_b) + \frac{m_t^2 - m_W^2}{m_W^2}(s^b(t)p_W)\right\}. \quad \text{(D15)}$$

[1] O. Buchmueller *et al.*, Eur. Phys. J. C **64**, 391 (2009).
[2] A. G. Cohen, D. B. Kaplan, and A. E. Nelson, Annu. Rev. Nucl. Part. Sci. **43**, 27 (1993).
[3] M. B. Gavela, P. Hernandez, J. Orloff, O. Pene, and C. Quimbay, Nucl. Phys. **B430**, 382 (1994).
[4] V. A. Rubakov and M. E. Shaposhnikov, Usp. Fiz. Nauk **166**, 493 (1996) [Sov. Phys. Usp. **39**, 461 (1996)].
[5] S. Dimopoulos and D. W. Sutter, Nucl. Phys. **B452**, 496 (1995).
[6] T. Ibrahim and P. Nath, Rev. Mod. Phys. **80**, 577 (2008).
[7] J. R. Ellis, J. S. Lee, and A. Pilaftsis, J. High Energy Phys. 10 (2008) 049.
[8] Y. Kizukuri and N. Oshimo, Phys. Rev. D **46**, 3025 (1992).
[9] T. Ibrahim and P. Nath, Phys. Rev. D **58**, 111301 (1998).
[10] T. Ibrahim and P. Nath, Phys. Rev. D **61**, 093004 (2000).
[11] M. Brhlik, G. J. Good, and G. L. Kane, Phys. Rev. D **59**, 115004 (1999).
[12] S. Abel, S. Khalil, and O. Lebedev, Nucl. Phys. **B606**, 151 (2001).
[13] R. L. Arnowitt, B. Dutta, and Y. Santoso, Phys. Rev. D **64**, 113010 (2001).
[14] Y. Li, S. Profumo, and M. Ramsey-Musolf, J. High Energy Phys. 08 (2010) 062.
[15] J. S. Lee *et al.*, Comput. Phys. Commun. **156**, 283 (2004).
[16] J. S. Lee, M. Carena, J. Ellis, A. Pilaftsis, and C. E. M. Wagner, Comput. Phys. Commun. **180**, 312 (2009).
[17] F. Deppisch and O. Kittel, J. High Energy Phys. 09 (2009) 110.
[18] S. Kraml, arXiv:0710.5117.
[19] V. D. Barger, T. Han, T.-J. Li, and T. Plehn, Phys. Lett. B **475**, 342 (2000).
[20] J. L. Kneur and G. Moultaka, Phys. Rev. D **61**, 095003 (2000).
[21] O. Kittel, J. Phys. Conf. Ser. **171**, 012094 (2009).
[22] S. Hesselbach, in *Proceedings of the LCWS/ILC 2007 Workshop at DESY, Hamburg, Germany, 2007*, econf C0705302, SUS11 (2007).
[23] A. Bartl, E. Christova, K. Hohenwarter-Sodek, and T. Kernreiter, Phys. Rev. D **70**, 095007 (2004).
[24] P. Langacker, G. Paz, L.-T. Wang, and I. Yavin, J. High Energy Phys. 07 (2007) 055.
[25] J. Ellis, F. Moortgat, G. Moortgat-Pick, J. M. Smillie, and J. Tattersall, Eur. Phys. J. C **60**, 633 (2009).
[26] K. Kiers, A. Szynkman, and D. London, Phys. Rev. D **74**, 035004 (2006).
[27] A. Bartl, E. Christova, K. Hohenwarter-Sodek, and T. Kernreiter, J. High Energy Phys. 11 (2006) 076.
[28] F. F. Deppisch and O. Kittel, J. High Energy Phys. 06 (2010) 067.
[29] G. Moortgat-Pick, K. Rolbiecki, J. Tattersall, and P. Wienemann, J. High Energy Phys. 01 (2010) 004.
[30] E. Boos *et al.*, Eur. Phys. J. C **30**, 395 (2003).
[31] G. Weiglein *et al.* (LHC/LC Study Group), Phys. Rep. **426**, 47 (2006).
[32] H. K. Dreiner, O. Kittel, and A. Marold, Phys. Rev. D **82**, 116005 (2010).
[33] H. Dreiner, O. Kittel, S. Kulkarni, and A. Marold, Phys. Rev. D **83**, 095012 (2011).
[34] T. Nattermann, K. Desch, P. Wienemann, and C. Zendler, J. High Energy Phys. 04 (2009) 057.
[35] D. Atwood, S. Bar-Shalom, G. Eilam, and A. Soni, Phys. Rep. **347**, 1 (2001).
[36] V. M. Abazov *et al.* (D0 Collaboration), Phys. Rev. D **82**, 032001 (2010).
[37] T. Aaltonen *et al.* (CDF Collaboration), arXiv:1101.0034.
[38] G. A. Moortgat-Pick, H. Fraas, A. Bartl, and W. Majerotto, Eur. Phys. J. C **9**, 521 (1999).
[39] H. E. Haber, arXiv:hep-ph/9405376.

[40] J. S. Schwinger, Phys. Rev. **82**, 914 (1951).
[41] J. S. Schwinger, Phys. Rev. **91**, 713 (1953).
[42] K. Kawagoe, M. M. Nojiri, and G. Polesello, Phys. Rev. D **71**, 035008 (2005).
[43] B. K. Gjelsten, D. J. Miller, and P. Osland, J. High Energy Phys. 12 (2004) 003.
[44] M. M. Nojiri, G. Polesello, and D. R. Tovey, arXiv:hep-ph/0312317.
[45] M. M. Nojiri, G. Polesello, and D. R. Tovey, J. High Energy Phys. 05 (2008) 014.
[46] H.-C. Cheng, J. F. Gunion, Z. Han, G. Marandella, and B. McElrath, J. High Energy Phys. 12 (2007) 076.
[47] H.-C. Cheng, J. F. Gunion, Z. Han, and B. McElrath, Phys. Rev. D **80**, 035020 (2009).
[48] D. Casadei, R. Djilkibaev, and R. Konoplich, Phys. Rev. D **82**, 075011 (2010).
[49] A. J. Barr and C. G. Lester, J. Phys. G **37**, 123001 (2010).
[50] G. Brooijmans *et al.*, arXiv:1005.1229.
[51] W. Porod, Comput. Phys. Commun. **153**, 275 (2003).
[52] V. Khachatryan *et al.* (CMS Collaboration), Phys. Lett. B **698**, 196 (2011).
[53] J. B. G. da Costa *et al.* (Atlas Collaboration), arXiv:1102.5290.
[54] K. Nakamura *et al.* (Particle Data Group), J. Phys. G **37**, 075021 (2010).
[55] M. Bahr *et al.*, Eur. Phys. J. C **58**, 639 (2008).
[56] M. Bahr *et al.*, arXiv:0812.0529.
[57] A. D. Martin, W. J. Stirling, R. S. Thorne, and G. Watt, Phys. Lett. B **652**, 292 (2007).
[58] P. Richardson, J. High Energy Phys. 11 (2001) 029.
[59] A. Buckley *et al.*, arXiv:1003.0694.
[60] B. M. Waugh *et al.*, arXiv:hep-ph/0605034.
[61] M. Cacciari and G. P. Salam, Phys. Lett. B **641**, 57 (2006).
[62] M. Cacciari, G. P. Salam, and G. Soyez, J. High Energy Phys. 04 (2008) 063.
[63] G. Aad *et al.* (ATLAS Collaboration), arXiv:0901.0512.
[64] J. Alwall *et al.*, J. High Energy Phys. 09 (2007) 028.
[65] K. Desch, J. Kalinowski, G. Moortgat-Pick, K. Rolbiecki, and W. J. Stirling, J. High Energy Phys. 12 (2006) 007.
[66] W. Beenakker, R. Hopker, and M. Spira, arXiv:hep-ph/9611232.
[67] W. Beenakker, R. Hopker, M. Spira, and P. M. Zerwas, Nucl. Phys. **B492**, 51 (1997).
[68] W. Beenakker, M. Kramer, T. Plehn, M. Spira, and P. M. Zerwas, Nucl. Phys. **B515**, 3 (1998).
[69] M. Lamont, LHC Near and Medium Terms Prospects, http://indico.desy.de/getFile.py/access?contribId=8&sessionId=15&resId=1&materialId=slides&confId=1964.
[70] F. Zimmermann, LHC beyond 2020, http://accnet.lal.in2p3.fr/Tasks/Literature/2010/KEK-Accelerator-Seminar-14July2010-LHC-Beyond-2020-Frank-Zimmermann.pdf.
[71] J. R. Ellis and S. Rudaz, Phys. Lett. B **128**, 248 (1983).
[72] H. E. Haber and G. L. Kane, Phys. Rep. **117**, 75 (1985).
[73] A. Bartl, H. Fraas, and W. Majerotto, Nucl. Phys. **B278**, 1 (1986).
[74] K. Rolbiecki, J. Tattersall, and G. Moortgat-Pick, Eur. Phys. J. C **71**, 1517 (2011).
[75] S. Y. Choi, H. S. Song, and W. Y. Song, Phys. Rev. D **61**, 075004 (2000).
[76] M. Fischer, S. Groote, J. G. Korner, and M. C. Mauser, Phys. Rev. D **65**, 054036 (2002).
[77] C. Amsler *et al.* (Particle Data Group), Phys. Lett. B **667**, 1 (2008).